



LITERATURE SURVEY

Physiologically Based Pharmacokinetic Modeling: Principles and Applications

LEONARD E. GERLOWSKI and RAKESH K. JAIN *

Received March 25, 1982, from the *Department of Chemical Engineering, Carnegie-Mellon University, Pittsburgh, PA 15213.*

Pharmacokinetic models are used to describe the time-dependent distribution and disposition of a substance in a living system and, as such, have numerous uses in clinical applications and drug design. For medicinal purposes, pharmacokinetics can be used to estimate optimal drug scheduling and dosage regimens. For industrial toxins, pharmacokinetics can be used to aid in determining safe working environments. The modeling procedure is useful in animal and clinical applications, and for obtaining fundamental knowledge of the transport and metabolism of a substance *in vivo*. In this paper we present a review of physiologically based pharmacokinetics in the hope of understanding and increasing the use of this modeling technique. Recent review articles on the subject have primarily focused on the use of physiologically based pharmacokinetics in cancer treatment. The most comprehensive of these articles discusses proper formulation of a model and development of the equations in detail (1). Other reviews on the subject discuss the application of this modeling technique to certain chemotherapeutic agents (2, 3). We present a rather extensive compilation of the literature on all substances modeled to date with this technique and discuss formulation of the equations, limitations of the modeling process, and areas of future applications to provide a unified framework for the understanding of physiologically based pharmacokinetics.

BACKGROUND

The term pharmacokinetics refers to prediction of the time-dependent concentrations of a substance in a living system. Two approaches currently in use are based on classical and physiological models. The classical approach utilizes a lumped-compartmental system and fits exponential functions to time-dependent plasma concentration data. The physiologically based approach separates the

body into a number of anatomical compartments, each compartment interconnected through the body fluid systems. The physiologically based approach also has the advantages of interspecies scalability, specific organ metabolism, specific organ transport, and specific organ binding properties.

Classical pharmacokinetic techniques are used to describe drug uptake with one- or multiple-compartmental systems. The solutions of differential equations that describe the time-dependent concentration behavior of the system consist of a series of decaying exponentials. The coefficients of the exponentials are fit to plasma, urinary, or some other obtainable tissue concentration data (4). Although these models are useful in many clinical situations (5), this modeling procedure does not describe a physiological system with large tissue-to-tissue concentration differences. In instances where the drug concentration is of the same order of magnitude over a large number of body organs, or certain other constraints are satisfied, a multiple-organ body system may indeed be simplified to a two-compartment model (6). For example, this intercompartmental variation is tolerable for drugs with a low therapeutic index; but substances that show high affinities for certain organs, are toxic to certain tissues, or have a specific target organ are not well described by the classical pharmacokinetic modeling technique (7).

The uptake of a drug is known to be dependent on organ perfusion rate, tissue volume, and many other biochemical and physiological parameters. The physiological parameters such as tissue volume, *etc.*, are scalable from species to species by a proportionality constant times body weight to some power (8, 9). If the uptake mechanisms are similar in small and large species, the biochemical and physiochemical parameters should be scalable through the species. However, the parameters obtained from classical

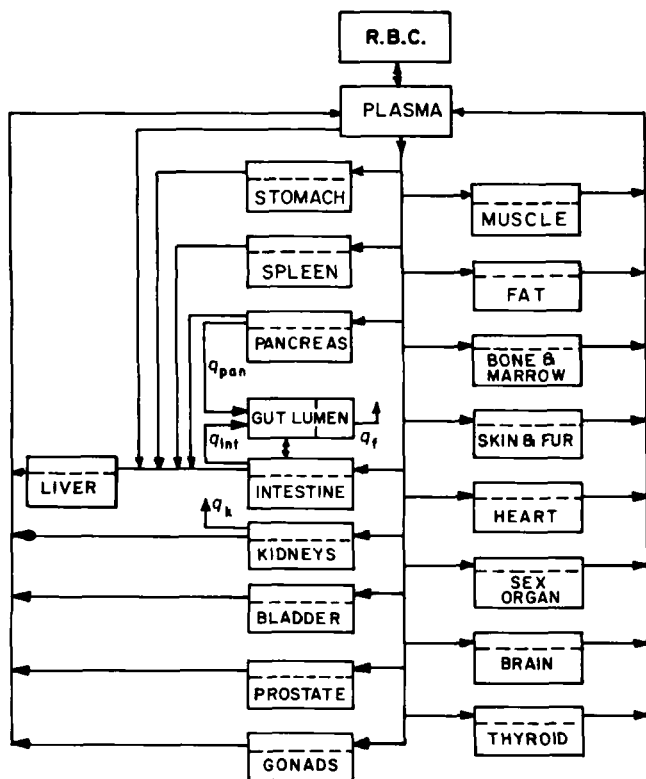


Figure 1—Example of a comprehensive physiologically based pharmacokinetic model flow scheme (15). Reprinted from the *Annals of Biomedical Engineering* with permission; copyright 1982, Pergamon Press, Ltd.

pharmacokinetics contain little physiological basis and, hence, show no scalability from species to species. Therefore, to describe a highly toxic substance with classical pharmacokinetics, all experimentation must be performed on a particular species (e.g., humans). The ability to scale-up a model to humans based on experiments with smaller species (mice, rats, dogs, etc.), could lead to the safer use of drugs.

The limitations of the classical approach have led to the need for a physiologically based approach. The first use of physiological parameters in modeling appeared in the 1930's when Teorell (10) included mass balances on specific tissues, with specific tissue volume and specific organ perfusion rates. In 1960, Bellman *et al.* (11) included capillary, interstitial, and cellular subcompartments in the modeling of drug distribution in organs. In this work, a perfused compartment with vascular, interstitial, and cellular spaces was solved analytically and applied to chemotherapy (11). In the late 1960's, Bischoff and Brown proposed a model which adapted and extended these ideas to predict drug distribution in mammals (12). This approach was later improved to describe time-dependent concentration profiles in various organs and interspecies scale-up. This physiologically based modeling technique has since been applied to numerous substances with much success.

DEVELOPMENT OF A MODEL

Compartmental analysis of a system requires a rational basis for selection of the size and number of compartments. In the classical pharmacokinetic approach, certain tissues of the body are lumped together to form one large com-

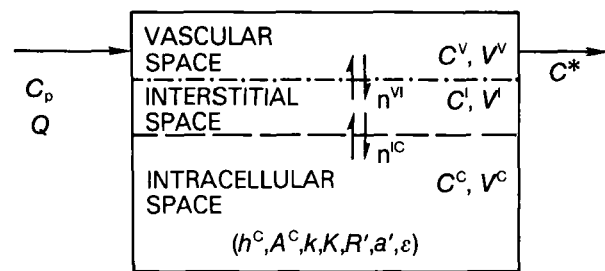


Figure 2—Schematic representation of the vascular, interstitial, and intracellular spaces of an organ. The flux of the substance occurs across the dashed lines; the arrows represent the direction of blood flow.

partment (such as a rapidly equilibrated compartment). The physical existence of such compartments does not realistically occur and is not easily visualized (13). In physiologically based pharmacokinetics, each compartment represents a particular organ or tissue and has anatomical significance. One approach in physiologically based pharmacokinetic modeling would be to model a whole body by performing mass balances on each organ and tissue. However, besides the cost of developing such an extensive model, such detailed distribution information is not required for most substances. For example, certain substances are known to accumulate primarily in a few organs [e.g., cadmium accumulates primarily in the liver and kidneys (14)]. Other substances are specifically toxic to certain organs (e.g., doxorubicin is a known cardiotoxin). Still other agents are desired to be toxic to a specific tissue (e.g., anticancer agents to tumors) or are desired to accumulate in a target organ (e.g., general anesthetics in the nervous system). This information is applied with physiological (tissue volumes and blood flow rates), physicochemical (binding, lipid solubility, ionization, etc.), and pharmacological (mechanism of transport, sites of action, etc.) knowledge of the substance in the body to simplify the model.

In the development of a physiological model, a flow scheme is assumed with the desired organs describing the species anatomically. Figure 1 is an interpretation of the circulatory flow scheme of a rat used to describe zinc uptake (15). Each organ is represented by a compartment, and all compartments are interconnected through the circulatory system as in the body. The physiological basis is maintained in the enterohepatic system with the liver, gut, spleen, and pancreas interconnected anatomically. Also, the substance is transferred from the liver to the gut lumen by the biliary system. The large number of organs incorporated in this flow scheme represents an attempt to develop a comprehensive model.

Each compartment is considered to consist of three well-mixed phases (referred to as subcompartments): (a) a vascular section through which the compartment (organ) is perfused with blood; (b) an interstitial space in the tissue which forms a matrix for the tissue cells; and (c) a cellular space consisting of the tissue cells that comprise the compartment (organ). This type of compartment is shown schematically in Fig. 2. Following injection, *via* any route of administration, the uptake of the substance in the compartment occurs through influx with the afferent blood in the vascular subcompartment. Each subcompartment is considered to be a well-mixed phase; therefore, the efferent blood has the same concentration as the vascular

subcompartment. The substance crosses the capillary wall and diffuses into the interstitial subcompartment. Then, the substance moves across the cellular membrane from the interstitial fluid into the cells. In each of the subcompartments, the agent may degrade by metabolic action or bind to an endogenous substance. Specific binding to a particular enzyme or cellular component may occur to allow for the therapeutic or toxic action of the agent. To form the model, mass balance equations on the substance in vascular, interstitial, and cellular subcompartments of organ i , respectively, are written as:

$$V_i^y \frac{dC_i^y}{dt} = Q_i C_p - Q_i C_i^y - n_i^{y-1} \quad (\text{Eq. 1})$$

$$V_i^I \frac{dC_i^I}{dt} = n_i^{y-1} - n_i^{I-C} \quad (\text{Eq. 2})$$

$$V_i^C \frac{dC_i^C}{dt} = n_i^{I-C} \quad (\text{Eq. 3})$$

The flux (n_i) in the above equations is used to describe either passive or carrier-mediated transport across the capillary wall (n_i^{y-1}) or cellular membrane (n_i^{I-C}). These mass balance equations are written for each organ. A mass balance on the substance is made on the plasma compartment to close the balance on the system:

$$V_p \frac{dC_p}{dt} = \sum_i Q_i C_i^y - Q_p C_p + g(t) \quad (\text{Eq. 4})$$

where $g(t)$ is the intravenous injection function. The mathematical form of $g(t)$ will depend on the form of injection, e.g., pulse, step input (16, 17). Injection into some other area of the body can easily be incorporated in such a model. These equations (Eqs. 1-4) are simplified in that metabolism, transport, binding, and excretion terms are not included. These processes are described in detail later in this article.

The uptake of a substance in a system thus can be described by a set of equations modeling the drug uptake in each subcompartment as a function of time. Although these subcompartments have a physiological basis, it is possible to measure reliably only total tissue concentration. [Jain *et al.* measured the concentration of methotrexate in the tumor interstitial fluid (18).] The total compartment (organ) concentration, C_i , thus is described by volume averaging the subcompartment concentrations:

$$C_i = \frac{C_i^y V_i^y + C_i^I V_i^I + C_i^C V_i^C}{V_i} \quad (\text{Eq. 5})$$

Flow Limitation (One Compartment)—When one of the steps in mass transfer is rate limiting, a compartment may be simplified from the three-subcompartment model to a model with one or two subcompartments. The flow-limited assumption to mass transfer is made for organs not well perfused by the circulatory system. This assumption implies that the transfer across the capillary wall and across the cellular membrane is very rapid when compared with the perfusion rate of the tissue. In essence, the vascular, interstitial, and cellular subcompartments are in equilibrium, and the mass balance on the compartment is written as:

$$V_i \frac{dC_i}{dt} = Q_i \left(C_p - \frac{C_i}{R_i} \right) \quad (\text{Eq. 6})$$

The term R_i in Eq. 6 is the partition coefficient and is the ratio of the drug concentration in the tissue to the drug concentration in the plasma at equilibrium.

Membrane Limitation (Two Subcompartments)—Another simplification occurs when the transfer across the cell membrane is the rate-limiting step; a two-subcompartmental model is assumed for the tissue. The two subcompartments are the cellular space, which consists of the tissue cells, and the extracellular space, which consists of the vascular and interstitial subcompartments in equilibrium, separated by a cellular membrane across which transport occurs. A mass balance on the extracellular space is:

$$V_i^E \frac{dC_i^E}{dt} = Q_i (C_p - C_i^E) - n_i^{E-C} \quad (\text{Eq. 7})$$

The flux across the cell membrane (n_i^{E-C}) accounts for net transfer to the cellular space; therefore, the accumulation in the cellular space can be described as:

$$V_i^C \frac{dC_i^C}{dt} = n_i^{E-C} \quad (\text{Eq. 8})$$

Again, the concentration of the whole organ (tissue) is volume averaged as:

$$C_i = \frac{V_i^E C_i^E + V_i^C C_i^C}{V_i} \quad (\text{Eq. 9})$$

Thus, Eqs. 7-9 and Eq. 4 are written over the system of organs to describe a complete mass balance of the agent being studied.

If the limitation to transfer of the agent is across the capillary wall, then the transfer is assumed to be capillary membrane limited. In this instance, the interstitial and cellular spaces are assumed in equilibrium, and a two-subcompartmental model is obtained similar to the cell membrane limitation. Equations similar to Eqs. 7-9 are written for the vascular and extravascular spaces to describe such organs.

Transport Mechanism—The transport of a substance across a biological membrane is complex and may occur by passive diffusion, carrier-mediated transport, or both (19). Here, we discuss the mathematical formulation of two simple cases. For the case of passive diffusion the flux across the cell membrane is described by a mass transfer coefficient (h_i) times a concentration driving force:

$$n_i^{E-C} = h_i \left(C_i^E - \frac{C_i^C}{R_i} \right) \quad (\text{Eq. 10})$$

However, in many biological systems the transport across a cell membrane is facilitated by carrier molecules. When this is the case, the flux is described by a saturable form:

$$n_i^{E-C} = \frac{a_i C_i^E}{b_i + C_i^E} - \frac{\frac{a_i C_i^C}{R_i}}{b_i + \frac{C_i^C}{R_i}} \quad (\text{Eq. 11})$$

When both transport mechanisms exist, the flux term is a linear combination of Eqs. 10 and 11.

For more in-depth studies on transport mechanisms, the reader is referred to treatises on the subject (20, 21).

Binding—Substances are known to bind to plasma,

interstitial, or subcellular proteins, and red blood cells and many other biological components. Details of binding can be found elsewhere (22, 23), but one simple case will be discussed. Binding of most substances follows a Langmuir-type isotherm, and the total amount of drug in a compartment can be expressed as the sum of the free and bound drug:

$$C_i = C_i^* + \frac{a_i C_i^*}{\epsilon_i + C_i^*} \quad (\text{Eq. 12})$$

which can be solved for the free drug concentration (C_i^*). When binding occurs in a subcompartment, only the free agent is available for mass transfer.

Excretion—The excretion of the agent must be taken into account to maintain a complete mass balance of the agent. For compartments such as the liver and kidneys, biliary and urinary excretion must be included, respectively. For example, Eq. 6 for a flow-limited compartment is modified to include an excretion rate term q_i (amount of drug excreted per unit time):

$$V_i \frac{dC_i}{dt} = Q_i \left(C_p - \frac{C_i}{R_i} \right) - q_i \quad (\text{Eq. 13})$$

In many cases, the excretion process can be described by a first-order approximation:

$$q_i = k_i C_i \quad (\text{Eq. 14})$$

In some cases, the plasma concentration is used instead of the tissue concentration. The linearity constant can be estimated from experimental data; the fraction of the initial dose excreted over a given amount of time (t_0) must satisfy the following equation:

$$(\text{fraction excreted}) \times (\text{initial dose}) = \int_0^{t_0} k_i C_i dt \quad (\text{Eq. 15})$$

If the excretion kinetics are assumed to be saturable, then:

$$q_i = \frac{v_{\max} C_i}{K_e + C_i} \quad (\text{Eq. 16})$$

The Michaelis–Menten constant must be determined by fitting the model to the excretion data.

Metabolism—In many biological environments, an agent is unstable and may be altered by chemical reaction. This degradation or change of the agent, referred to as metabolism, must be taken into account to completely describe the distribution and disposition of an agent. In specific instances, the metabolite may be the actual agent of interest (24). The metabolism of an agent in the model is described by a reaction rate [$r_i(t)$]. In most cases of interest, the metabolism reactions are assumed to follow either first-order or Michaelis–Menten saturable kinetics. For first-order kinetics in a flow-limited compartment i , Eq. 6 would become:

$$V_i \frac{dC_i}{dt} = Q_i \left(C_p - \frac{C_i}{R_i} \right) - k_i C_i \quad (\text{Eq. 17})$$

For Michaelis–Menten kinetics, Eq. 6 would be:

$$V_i \frac{dC_i}{dt} = Q_i \left(C_p - \frac{C_i}{R_i} \right) - \frac{C_i v_{\max}}{K_m + C_i} \quad (\text{Eq. 18})$$

The order, rate, and rate constants for metabolism are normally determined from *in vitro* studies. Whenever possible, these *in vitro* rate constants are used to describe metabolism *in vivo*. On many occasions the metabolism of a drug occurs primarily in a particular organ for which the kinetic data may not be readily available. In these instances the constants are obtained as best-fit parameters to pharmacokinetic data. Based on the flow-, capillary-, or membrane-limitation assumptions, equations similar to those of the parent compound are written to describe the pharmacokinetics of the metabolites.

Parameter Estimation—Time-dependent concentration data are obtained from laboratory animals sacrificed at predetermined intervals following an injection. To describe these data, the model parameters must be specified or estimated. The physiological parameters such as blood flow rate (Q_i) and tissue volume (V_i) can be determined from various experimental methods. For most species these values can be readily found in the literature. Kinetic parameters may be determined from separate experiments *in vivo* or *in vitro*. In some cases, the tissue-to-plasma binding constants are measured experimentally following long-term constant infusion. In other cases, the binding constants (R_i) and the passive diffusion coefficients (h_i) are estimated from the long- and short-term data, respectively (25), following a pulse injection. If *in vivo-in vitro* correlations are not available or appropriate, these parameters are determined from best fits of the concentration profile simulations to tissue concentration data. Once all parameter values are specified, the coupled, ordinary, and sometimes nonlinear first-order differential equations which describe the mass balance on the system need to be solved numerically to simulate the data (28).

For details of parameter estimation the reader is referred elsewhere (26, 27).

MODELS FOR SPECIFIC AGENTS

The pharmacokinetics of many substances have been described by this modeling technique. We have divided these models into six categories: (a) anticancer agents, (b) antibiotics, (c) anesthetics, (d) single elements (trace metals and ions), (e) environmental hazards and toxic substances, and (f) others. We realize that in this classification system, some anticancer agents are also antibiotics. Table I is an outline of 37 substances indicating the molecular structure, biological action, several treatment usages (for anticancer agents), the species modeled, and comments about the assumptions and limitations of the particular model. These models are described in more detail in the following section. The physiological parameters for each species are listed in Table II; the physicochemical and biological parameters for each model are tabulated throughout the text.

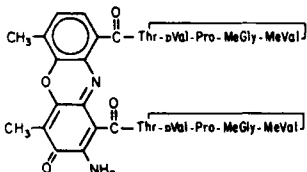
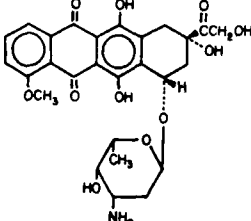
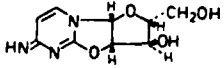
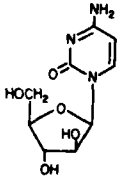
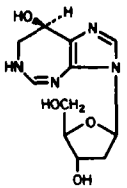
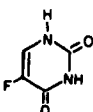
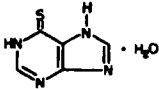
Anticancer Agents—Most drugs used to treat cancer are toxic to both normal and neoplastic tissues. These drugs are used for therapy in various dosages and schedules, usually given in combination with other antineoplastic agents to obtain optimal therapeutic effects in cancer patients. The high toxicity of these drugs makes it desirable to quantify their intake, distribution, metabolism, and excretion in various tissues of the body. To this extent, physiologically based pharmacokinetics has been

applied to study these processes. These models may be useful in estimating dosages and schedules which ensure that tissue concentrations remain below the toxic level for normal tissue and above the toxic level for neoplastic tissue. Initially, these models are developed for small animals and then scaled-up to humans in hopes of being able to prescribe dosage levels and administration schedules that ensure patient safety and optimal drug usage.

Dactinomycin—Actinomycin is a naturally occurring crystalline antibiotic of which all forms have been syn-

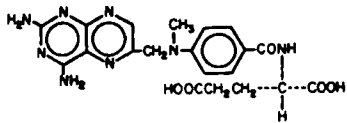
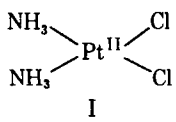
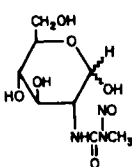
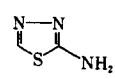
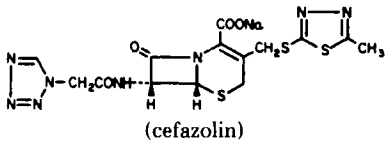
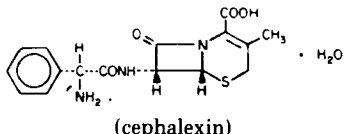
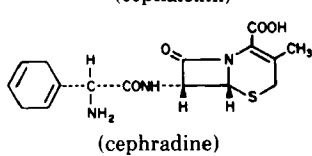
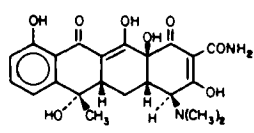
thesized. Dactinomycin (actinomycin D) has been used to treat various neoplasms, including gestational carcinoma, testicular neoplasm, and Wilms tumor. The mechanism of action of dactinomycin includes binding to DNA, thus preventing progression of RNA polymerase along the DNA template. Lethal damage from dactinomycin occurs along the intestinal mucosa. A flow-limited physiologically based pharmacokinetic model was developed by Lutz *et al.* to describe the distribution of dactinomycin in the beagle dog (29) at doses of 0.03 and 0.135 mg/kg iv. The 13-compart-

Table I—Agents Modeled by Physiologically Based Pharmacokinetics

Agent	Chemical Structure	Biological Effect ^a	Reference	Model Species	Comments
Chemotherapeutic Agents					
Dactinomycin		-blocks RNA synthesis by binding to DNA -gestational carcinoma, testicular neoplasm, Wilms tumor	(29)	dog	Flow and diffusion limitation
Doxorubicin		-binds to DNA, interferes with DNA function and RNA synthesis -acute lymphoblastic and acute myeloblastic leukemias, Wilms tumor, neuroblastoma, breast and ovarian carcinomas	(31) (32) (34) (33)	rabbit, human human hamster mouse	Flow limited Applied previous model (31) to human Membrane limited Membrane limited with flow-limited tumor
Ancitabine		-leukemia	(24)	human	Flow limited, Michaelis-Menten kinetics
Cytarabine		-blocks DNA synthesis and introduces moieties into the DNA coding sequence -ovarian cancer	(35) (36) (38)	human mouse, dog, monkey mouse	Flow limited, nonlinear metabolism Flow limited, nonlinear metabolism Extends Dedrick model (37) to include intracellular metabolism
Pentostatin		-binding inhibitor of adenosine deaminase -leukemia	(39)	mouse	Flow limited
5-Fluorouracil		-anabolic: blocks the methylation reaction of deoxyuridylic acid to thymidylic acid, interferes with DNA synthesis; catabolic: degeneration to CO ₂ and urea -carcinomas of the colon, rectum, breast, stomach, and pancreas	(40)	rat	Flow limited, saturable excretion, hybrid model
Mercaptopurine		-acute lymphocytic leukemia	(42)	rat	Flow limited

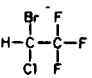
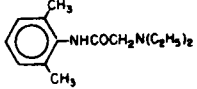
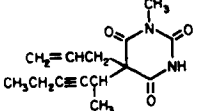
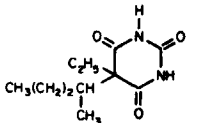
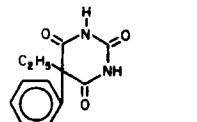
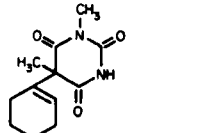
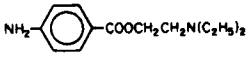
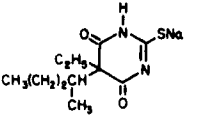
Continued on next page

Table I-Continued

Agent	Chemical Structure	Biological Effect ^a	Model		
			Reference	Species	Comments
Methotrexate		-strongly binds to intracellular dihydrofolate and inhibits conversion to tetrahydrofolate (an inhibitor in DNA synthesis) -leukemia, lung tumor, choriocarcinoma, Burkett's lymphoma	(44)	mouse	Flow limited, nonlinear
			(43)	mouse, rat, dogs, monkey, human	Flow limited, nonlinear excretion
			(45)	sting ray	Flow limited
			(25)	rat	Membrane limited, nonlinear transport
			(46)	mouse	Flow limited, hybrid model
			(47)	dog	Hybrid model, nonlinear transport
			(48)	mouse	Hybrid model, membrane limited
			(37)	human	Membrane limited, nonlinear transport
Cisplatin		-produces intra- and interstrand crosslinks in DNA -metastatic testicular and ovarian tumors	(50)	dog	Flow limited, linear binding, first-order metabolism
Streptozocin		-inhibits DNA synthesis by alkylation of cell components -pancreatic tumor	(51)	mouse	Membrane limited
2-Amino-1,3,4-thiadiazole		-inhibits the action of inosine-5-phosphate dehydrogenase in leukemia cells -melanoma, glioblastoma, lymphosarcoma, leukemia	(52)	mouse, dog, monkey	Flow limited, linear and saturable metabolism
Cephalosporins	 <p>(cefazolin)</p>	-antibiotic	(53)	human	Flow limited
	 <p>(cephalexin)</p>				
	 <p>(cephadrine)</p>				
Tetracycline		-antibiotic; exhibits maternal and fetal toxic effects	(16)	rat	Flow limited with placenta compartment
β -Lactam antibiotics	(various)	-antibiotic	(54)	rat	Flow and membrane limited, linear and nonlinear binding (depending on drug)

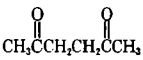
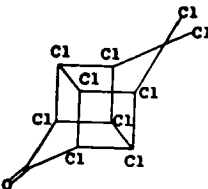
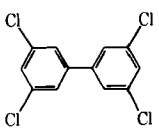
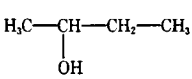
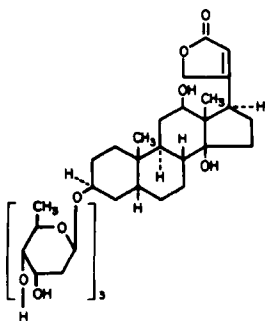
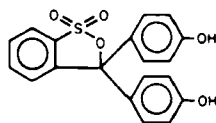
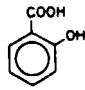
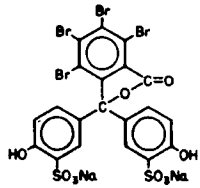
continued

Table I-Continued

Agent	Chemical Structure	Biological Effect ^a	Model		
			Reference	Species	Comments
<u>Anesthetics</u>					
Halothane		-general anesthetic	(57)	human	Nonlinear Flow limited Flow limited Nonlinear, flow limited
			(17)	human	
			(58)	human	
			(59)	human	
Lidocaine		-local anesthetic	(65)	monkey, human	Flow limited
Methohexital		-short-acting, local anesthetic	(63)	human	Nonlinear
Pentobarbital		-sedative, anticonvulsant	(61)	human	Application of the thiopental model to humans
Phenobarbital		-anticonvulsant, hypnotic, sedative	(64)	rat	Flow limited
Hexobarbital		-hypnotic, sedative	(64)	rat	Flow limited
Procaine		-local anesthetic	(67)	human	Nonlinear binding and metabolism, flow limited
Thiopental sodium		-local anesthetic	(60)	dog, human	Flow limited, nonlinear Flow limited Flow limited, nonlinear metabolism and binding Nonlinear Flow limited
			(61)	dog, human	
			(62)	dog	
			(63)	human	
			(64)	human	
			<u>Trace Metals and Other Ions</u>		
Bromide	Br ⁻	-toxic at high doses leading to mental and neurological disorders -used to measure extracellular space	(69)	rat	Flow and membrane limited
Cadmium	Cd	-toxic at high doses leading to hypertension and necrosis of testicles	(73)	mouse	Flow and membrane limited
Chloride	Cl ⁻	-essential electrolyte, osmotic balance gastric hydrochloride	(74)	cat	Flow limited
Lithium	Li ⁺	-potentially toxic at high doses -preferred drug for treating manic-depressive illness	(75)	human	Nonlinear uptake
Zinc	Zn	-essential trace element for DNA and protein synthesis -effects carbohydrate metabolism, lipid peroxidation, bone formation	(15)	rat	Membrane limited

continued on next page

Table I—Continued

Agent	Chemical Structure	Biological Effect ^a	Model		
			Reference	Species	Comments
<u>Environmental Hazards and Toxic Substances</u>					
Acetylacetone		-neurotoxic	(76)	mouse	Flow limited
Chlordecone		-toxic	(78)	rat	Membrane limited
Nitrite	(CH ₃) ₂ NNO (<i>n</i> -nitrosodimethylamine)	-carcinogenic	(79)	human	Accounts for nitrite formed endogenously to the carcinogen nitrosamine
Polychlorinated biphenyls		-environmental contaminants, possible toxicants	(80)	rat	Flow limited
		-accumulation in adipose tissue	(81)	rat	Flow limited, includes
			(82)	rat	Flow limited
<u>Others</u>					
2-Butanol		-pretreatment can potentiate the toxicity of carbon tetrachloride	(83)	rat	Flow limited, metabolites, nonlinear metabolism, oral administration
Digoxin		-cardiotonic: increases myocardial contraction force;	(84)	rat	Flow limited
		depressant: decreases cardiac rate	(85)	dog, human	Flow limited
Ethanol	H ₃ C—CH ₂ —OH	-depressant	(86)	rat	Hybrid, flow limited
			(87)	dog	Hybrid, flow limited
Phenolsulfonphthalein		-renal function test	(88)	shark	Flow limited
Salicylates	 (salicylic acid)	-antipyretic and analgesic	(89)	dog	Flow limited, Michaelis-Menten metabolism
Sulfobromophthalein		-liver function test	(90)	rat, human	Flow limited
			(91)	rat	Flow limited
Tetraethylammonium ion	(C ₂ H ₅) ₄ N ⁺	-ganglion blocking agent, antihypertensive, peripheral vasodilator	(92)	rat	Membrane limited, nonlinear

^a Biologic mechanism and several uses (treatments).

Table II—Physiological Parameters

Parameter	Mouse ^a	Hamster ^b	Rat ^c	Rabbit ^d	Monkey ^a	Dog ^e	Human ^f
Body weight, g	22	150	500	2330	5000	12,000	70,000
Volume, ml							
Plasma	1.0	6.48	19.6	70	220	500	3000
Muscle	10.0	—	245	1350	2500	5530	35,000
Kidney	0.34	1.36	3.65	15	30	60	280
Liver	1.3	6.89	19.55	100	135	480	1350
Gut	1.5	12.23	11.25	120	230	480	2100
Gut Lumen	1.5	—	8.8	—	230	—	2100
Heart	0.095	0.63	1.15	6	17	120	300
Lungs	0.12	0.74	2.1	17	—	120	—
Spleen	0.1	0.54	1.3	1	—	36	160
Fat	—	—	34.9	—	—	—	10,000
Marrow	0.6	—	—	47	135	120	1400
Bladder	—	—	1.05	—	—	—	—
Brain	—	—	—	—	—	—	1500
Pancreas	—	—	2.15	—	—	24	—
Prostate	—	—	6.4	—	—	—	—
Thyroid	—	—	0.85	—	—	—	20
Plasma Flow Rate, ml/min							
Plasma	4.38	40.34	84.6	520	379	512	3670
Muscle	0.5	—	22.4	155	50	138	420
Kidney	0.8	5.27	12.8	80	74	90	700
Liver	1.1	6.5	4.7	177	92	60	800
Gut	0.9	5.3	14.6	111	75	81.5	700
Heart	0.28	0.14	1.6	16	65	60	150
Lungs	4.38	28.4	2.25	520	—	512	—
Spleen	0.05	0.25	0.95	9	—	13.5	240
Fat	—	—	3.6	—	—	—	200
Marrow	0.17	—	—	11	23	20	120
Bladder	—	—	1.0	—	—	—	—
Brain	—	—	0.95	—	—	—	380
Pancreas	—	—	1.1	—	—	21.3	—
Prostate	—	—	0.5	—	—	—	—
Thyroid	—	—	0.8	—	—	—	20

^a Data (43) reprinted from the *Journal of Pharmaceutical Sciences* with permission; © 1971, American Pharmaceutical Association. ^b Data taken from Ref. 34. ^c Data (15) reprinted from the *Annals of Biomedical Engineering* with permission; © 1982, Pergamon Press, Inc. ^d Data taken from Ref. 31. ^e Data (29) reprinted from the *Journal of Pharmacology and Experimental Therapeutics* with permission; © 1977, American Society for Pharmacology and Experimental Therapeutics. ^f Data taken from Ref. 1.

mental model with linear binding in the tissue used the transport and binding parameters listed in Table III. The authors have compared the cell mass transfer coefficient with blood flow rate per unit volume of normal tissues and have found that both are of the same order of magnitude, thus indicating the appropriateness of the flow-limited assumptions. An exception to the flow-limited assumption was the testis compartment where the perfusion rate was much larger than the mass transfer coefficient, suggesting that the testes, analogous to the brain, have a low permeability membrane barrier. This result has important implications in the treatment of testicular neoplasms.

Doxorubicin—The anthracycline antibiotic doxorubicin hydrochloride¹ has been used in chemotherapeutic treatment of various solid tumors, lymphomas, and sarcomas (e.g., acute lymphoblastic and myeloblastic leukemia, Wilms tumor, neuroblastoma, breast carcinoma, ovarian carcinoma). Doxorubicin exhibits neoplastic effects through interference with DNA functions and RNA synthesis. However, recent studies indicate that binding of the drug to cell membranes may be the lethal step (30). Toxic effects include depression of cell production in bone marrow and dose-dependent cardiomyopathy, thereby limiting dosages to low levels. To this end, Harris and Gross have modeled doxorubicin pharmacokinetics in the rabbit (31), Chan *et al.* in humans (32), Townsend in the hamster (33), and Gerlowski in the mouse (34) (Table IV). The rabbit model of Harris and Gross contains 10 flow-limited compartments. Their model overestimates con-

Table III—Model Parameters for Dactinomycin in the Dog^a

Compartment	Flow-Limited Binding Constant (R)	Membrane Limited	
		Mass Transfer Coefficient (h), hr ⁻¹	Drug-DNA Dissociation Constant (D), µg/ml
Lung	53	7.7	0.5
Heart	11	7.7	0.5
Spleen	55	7.7	0.5
Stomach	25	7.7	0.5
GI tract	42	7.7	0.5
Liver	30	7.7	0.5
Kidney	45	7.7	0.5
Testes	18	0.2	0.5
Salivary gland	44	7.7	0.5
Thymus	47	7.7	0.5
Bone marrow	20	7.7	0.5
Pancreas	45	7.7	0.5
Muscle	8	7.7	0.5

^a Data (29) reprinted from the *Journal of Pharmacology and Experimental Therapeutics* with permission; © 1977, American Society for Pharmacology and Experimental Therapeutics.

centration data at times <5 hr, indicating that a diffusion limitation may exist. These authors have also compared the model simulations with human plasma data and found underprediction at early intervals and overprediction at 24–48 hr. Chan *et al.* adapted the Harris and Gross model to simulate human plasma data. The authors were able to show consistent agreement with normal patients and, in some cases, in patients with significant hepatic dysfunction who show prolonged doxorubicin levels. The human plasma data also exhibited a short-term (2–4 hr) behavior not predicted by a flow-limited model, suggesting the need

¹ Adriamycin; Adria Laboratories, Columbus, Ohio.

Table IV—Model Parameters for Doxorubicin in the Human, Rabbit, Hamster, and Mouse

Tissue	Human ^a and Rabbit ^b	Hamster ^c		Mouse ^d	
	Linear Binding Constant (R) ^e	Mass Transfer Coefficient (h) ^f , min ⁻¹	Linear Binding Constant (R') ^f	Mass Transfer Coefficient (h) ^f , min ⁻¹	Linear Binding Constant (R') ^f
Plasma	0.5	—	—	—	—
Adipose tissue	19	—	—	—	—
Lean tissue	29	—	—	—	—
Liver	45	0.26	300	0.023	400
Gut	51	0.082	35	0.082	35
Heart	57	0.027	12	0.004	0.5
Bone marrow	91	—	—	—	—
Lungs	155	0.041	27	0.0009	7
Kidney	512	0.13	90	0.0044	1000
Spleen	556	0.046	40	0.046	40
Tumor	—	0.0075	15	—	0.5 ^e
Other values, ml/min					
k_{el}	70	—	—	—	—
Liver clearance (k_l)	—	0.011	—	0.0085	—
Kidney clearance (k_k)	—	0.0074	—	0.0004	—

^a Data taken from Ref. 32. ^b Data taken from Ref. 31. ^c Data taken from Ref. 33. ^d Data taken from Ref. 34. ^e Flow limited. ^f Membrane limited.

to incorporate metabolism and membrane-limited assumptions into such a model.

The mouse and hamster models contain seven organs, all membrane limited, except the tumor compartment in the mouse, which was assumed to be flow limited (33, 35). It is known that doxorubicin metabolizes primarily in the intracellular space. Since the metabolite has similar antineoplastic effects, it was lumped with the drug as doxorubicin equivalents in these models. Good agreement was obtained with both early- and late-interval data, supporting the existence of a membrane limitation. In addition to the lumped doxorubicin analysis, Townsend (33) tried to model the metabolism as saturable intracellular reactions in the liver and kidney using parameters determined *in vitro*. Although no comparison with data for the metabolite was shown, simulations indicate that the metabolite concentrations in the hamster are at least one order of magnitude below the parent drug concentration levels, in contrast to the human data.

Cytarabine—Cytarabine (ara-C) is a neoplastic agent which provides an excellent example of the usefulness of *in vitro* enzyme kinetics in physiologically based pharmacokinetic modeling. Cytarabine is known to metabolize in the liver *via* pyrimidine nucleotide deaminase to 1- β -D-furanosyluracil. For antineoplastic action, cytarabine must be phosphorylated to the nucleotide. It is the nucleotide that is considered to act as an inhibitor of DNA polymerase by incorporation into the DNA template. Cytarabine and its metabolites were modeled in the mouse, dog, monkey, and human by Dedrick *et al.* (35–37) and in the mouse by Morrison *et al.* (38). A six-compartment flow-limited model was developed by Dedrick *et al.* to describe cytarabine distribution and its metabolism to 1- β -D-furanosyluracil by saturable kinetics. This study was one of the first models in the literature to apply *in vitro* saturable kinetic parameters to describe *in vivo* human data (35). In physiologically based pharmacokinetics, models are usually developed for small animals and then scaled-up to humans. In this case, the human model was developed first and then extended to mice, monkeys, and dogs (36) to study interspecies differences in pharmacokinetic modeling. The kidney clearance constant was found to exhibit essentially the same variation with body weight as seen for inulin. This model was later extended by De-

drick *et al.* (37) to include a peritoneal cavity compartment and was used successfully to develop rational protocols to treat patients with ovarian cancer.

The model of cytarabine in the mouse by Morrison *et al.* (38) extends the Dedrick model to include intracellular metabolism of the drug to the active metabolite, arabinoside cytosine triphosphate. The authors applied *in vitro* reaction constants for saturable kinetics to determine cytarabine and triphosphate cytarabine concentration profiles in various tissues. The kinetics of this reaction are strain dependent (as shown in the mouse), perhaps due to different levels of liver deaminase among strains. When scaling-up to humans, these effects must be incorporated with the higher pyrimidine activity in human marrow (relative to other tissue sites) than in murine systems. Also, the Michaelis constant of human pyrimidine deaminase is much lower than that found in mice, thus increasing the importance of deoxycytine and cytidine as inhibitors. The results indicate quite different concentration profiles of these substances, suggesting that the kinetics of reaction must be determined for the prediction of DNA inhibition by these substances.

Ancitabine—Ancitabine (cycloctidine) is known to hydrolyze *in vivo* to the effective anticancer agent cytarabine. This drug is known to have a slower urinary clearance than cytarabine, by metabolism and kidney clearance, leading to an enhanced cytotoxic effect in tumor-bearing animals. Following the models of Dedrick *et al.* for cytarabine (35, 36), Himmelstein and Gross have developed a six-compartment model to predict this effect in humans (24). All compartments were assumed to be flow limited, and the hydrolysis reaction was considered to occur by saturable kinetics in all compartments. *In vitro*-determined values were used for hydrolysis rate constants, and clearance values were calculated from cumulative urinary data assuming linear excretion for both ancitabine and cytarabine (Table V). Based on good agreement with the plasma data in humans, the authors conclude that ancitabine can act as an *in vivo* reservoir for cytarabine, and therefore, its pharmacokinetics should be considered in developing treatment schedules.

Pentostatin—Pentostatin (2'-deoxycoformycin) is a bacterial fermentation product which is used primarily in combination chemotherapy with other antineoplastic

Table V—Model Parameters for Cytarabine in the Mouse, Monkey, Dog, and Human and Ancitabine in the Human

Parameter	Cytarabine ^a				Ancitabine ^b
	Mouse	Monkey	Dog	Human	Human
Michaelis constant (K_m), $\mu\text{g/ml H}_2\text{O}$	283	39	115	39	—
Heart	—	—	—	—	31
Liver	—	—	—	—	27
Kidney	—	—	—	—	32
Deaminase activity (v_{max}), $\mu\text{g/g}\cdot\text{min}$					
Blood	—	1.6	—	—	—
Liver	4.6	80.2	7	119	119
Gut	8.3	—	—	—	—
Heart	—	57	—	6	6
Kidney	91.5	71.8	—	20	20
Lean tissue	—	34.3	—	—	—
Kidney clearance (k_k), ml/min	0.18	14	32	90	90

^a Data (36) reprinted from *Biochemical Pharmacology* with permission; © 1973, Pergamon Press, Ltd. ^b Data (24) reprinted from the *Journal of Pharmaceutical Sciences* with permission © 1977, American Pharmaceutical Association.

agents. When applied with vidarabine (ara-A), increased antitumor activity is found in laboratory animals. Pentostatin is a tight-binding inhibitor of intracellular adenosine deaminase in the liver, kidney, and L-1210 tumor cells. King and Dedrick developed a five-compartment model to describe pentostatin pharmacokinetics in normal and leukemic mice (Table VI) (39). The authors used both linear and nonlinear binding in a flow-limited model to account for tissue distribution at high pentostatin concentrations and for the tight binding to adenosine deaminase, respectively. Since blood flow rate to L-1210 tumors is not known, these authors have estimated the blood flow rate to be 0.22 min^{-1} by fitting their model to the tumor data. Pharmacokinetic parameters for normal tissues were determined by decomposing the model into a series of hybrid models which could be solved individually. The model indicated that the primary means of drug elimination was through the urinary tract, although the model was not able to predict this data well at high dosages. These authors suggest that a more comprehensive model should include the detailed kinetics of the inhibition of adenosine deaminase by pentostatin and the dissociation rate of the pentostatin-adenosine deaminase complex based on experimental data.

5-Fluorouracil—The pharmacokinetics of 5-fluorouracil are of interest since the drug is known to be metabolized by two pathways in the body. The anticancer effect of 5-fluorouracil results from an anabolic pathway where the drug incorporates into nucleosides and nucleotides. A

Table VI—Model Parameters for Pentostatin in the Mouse^a

Tissue	Linear Binding Constant (R)	Dissociation Constant $\mu\text{g/ml}$	Specific Binding Parameter, $\mu\text{g/ml}$	
			Normal Mice	Leukemic Mice
Gut	1.0	0.7	82	101
Liver	1.24	0.7	18	61
Kidney	2.8	0.7	16	32
Tumor	0.72	0.7	—	92
Carcass	0.56	0.7	45	45
Other values, ml/min				
Glomerular filtration rate			0.30	0.26
Secretion clearance			0.35	0.30

^a Data (39) reprinted from the *Journal of Pharmacokinetics and Biopharmaceutics* with permission; © 1981, Plenum Publishing Corp.

Table VII—Model Parameters for Mercaptopurine in the Rat and Human^a

Tissue	Rat		Human	
	Linear Binding Constant (R)	Strong Binding Constant (a) $\mu\text{g/ml}$	Linear Binding Constant (R)	Strong Binding Constant (a), $\mu\text{g/ml}$
Muscle	1.4	0.0	1.4	0.0
Kidney	2.4	0.35	2.4	0.35
Liver	4.0	0.6	4.0	0.6
Gut	3.0	0.1	3.0	0.1
Spleen	1.7	0.2	1.7	0.2
Bone marrow	0.35	0.2	0.35	0.2
Other values				
Kidney clearance (k_k) ml/min		1.2		315
Biliary clearance (k_l) ml/min		1.2		500
Time constants				
bile duct (τ_B)		1.0		10
GI tract (τ_{GI})		100		1000

^a Data (42) reprinted from the *Journal of Pharmaceutical Sciences* with permission; © 1977, American Pharmaceutical Association.

catabolic pathway for metabolism also exists, where the drug undergoes degradation ultimately to carbon dioxide and urea. A two-compartment flow-limited hybrid model around the pulmonary system was developed by Collins *et al.* (40) for humans. The authors did not differentiate between the two metabolic pathways in the model, but presented a framework on which to build. The novel aspect of this work results from the route- and schedule-dependent drug clearance. The model included saturable clearances and was used for the intravenous bolus, intravenous infusion, and intraperitoneal injection routes. Because of the good fit to data for the different modes of administration, the authors concluded that the simple physiologically based pharmacokinetic model with nonlinear terms is sufficient for use in clinical situations.

Mercaptopurine—The primary use of mercaptopurine is in combination therapy for treatment of leukemia and certain sarcomas (41). Mercaptopurine is most toxic to rapidly multiplying cells; therefore, the intestine, bone marrow, and spleen are more susceptible to mercaptopurine and are of primary interest in the modeling of this drug. Tterlikkis *et al.* (42) have developed a six-compartment flow-limited model with a complete hepatic system to describe the pharmacokinetics of mercaptopurine in the rat (Table VII). The model, similar to one developed by Bischoff *et al.* (43), includes linear binding and excretion, a three-compartment biliary tract, and a four-compartment gut lumen. The rat concentration data were simulated well by the model. The authors also scaled-up their model to humans and have obtained general agreement with the data despite large patient-to-patient differences. A more comprehensive model of mercaptopurine should include detailed kinetics of metabolism analogous to the models for cytarabine, cisplatin, *etc.* When this kinetic framework is determined, a clinically applicable model can be made available based on the structure presented in this work.

Methotrexate—Methotrexate has been the most studied drug in the area of physiologically based pharmacokinetics. The antineoplastic mechanism of methotrexate results from its binding to the enzyme dihydrofo-

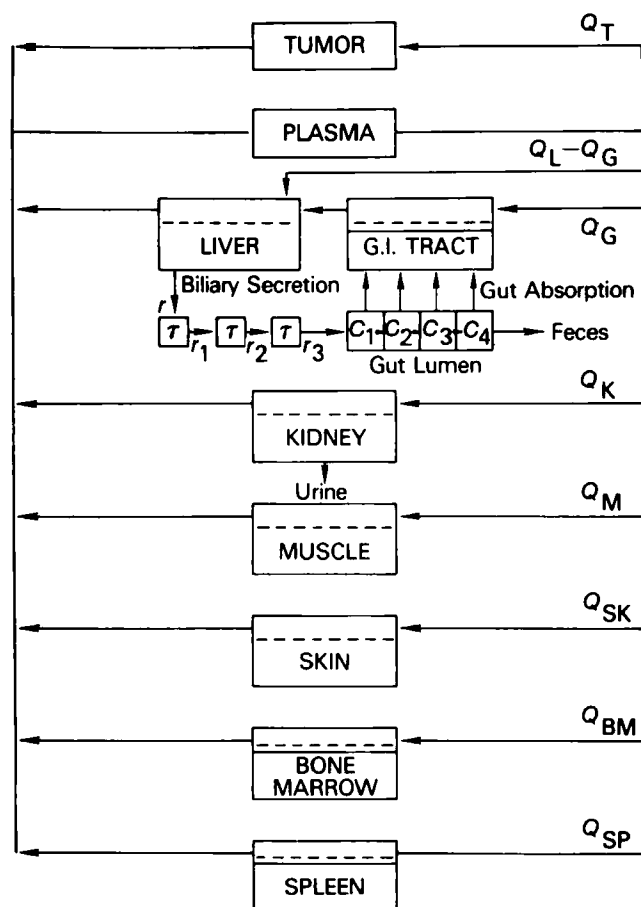


Figure 3—Location of the biliary and gut lumen compartments represented by well-mixed subcompartments connected in series.

late reductase which inhibits conversion of dihydrofolate to tetrahydrofolate. Tetrahydrofolate is used to produce a coenzyme required for thymidylate formation, which in turn, is required for DNA synthesis. Preliminary pharmacokinetic work on methotrexate began with a six-compartment model that was simplified to a two-compartment model by Bischoff *et al.* (43). The analytical solutions of this simple model were used to obtain initial estimates of mass transfer coefficients and clearance constants. The equations for the six-compartment flow-limited model were solved with a numerical technique, and good agreement with data for the six tissues was found.

Bischoff *et al.* then extended their model by incorporating saturable binding and excretion, multicompartmental representation of biliary excretion, and movement of drug through the GI tract with partial reabsorption (Fig. 3) (44). The model was able to predict successfully detailed distribution and excretion of methotrexate in the mouse, rat, monkey, dog, and human over a wide range of doses.

Dedrick *et al.* (25) determined membrane resistance to transport in bone marrow, the spleen, and the small intestine of rats by plotting the drug concentrations in various tissues as functions of the plasma concentration. The transport parameters estimated from the membrane-limited model were found to be in general agreement with *in vitro* results obtained in many mammalian cells. The mathematical treatment presented in this paper was general and has been adapted by many investigators of physiologically based pharmacokinetics.

Zaharko *et al.* (45) used the flow-limited model to pre-

Table VIII—Model Parameters for Methotrexate in the Mouse, Rat, Dog, Monkey, and Human ^a

Tissue	Linear Binding Constant (<i>R</i>)				
	Mouse	Rat	Monkey	Dog (5 kg)	Dog (17 kg) Human
Muscle	0.15	0.15	0.15	0.15	0.15
Kidney	3.0	3.0	14	14	3.0
Liver	10	3.0	2.0	2.0	3.0
Gut	1.0	1.0	1.0	1.0	1.0
Clearance rate, ml/min					
kidney (<i>k_k</i>)	0.2	1.1	20	56	190
bile (<i>k_b</i>)	0.4	3.0	2.0	8	200

^a Data (43) reprinted from the *Journal of Pharmaceutical Sciences* with permission; © 1971, American Pharmaceutical Association.

dict the distribution of methotrexate in the sting ray and found the blood circulation velocity to be approximately one-sixteenth of that in the mouse. Dedrick *et al.* (37) used the membrane-limited model to simulate plasma and peritoneal fluid concentrations following single and repeated intraperitoneal injections of methotrexate in humans. This work led to the conclusion that a significantly greater concentration of methotrexate in the peritoneal cavity than in the plasma following intraperitoneal injection could be exploited in the treatment of patients with microscopic residual cancer confined to the peritoneal cavity.

Zaharko *et al.* (46) and Lutz *et al.* (47) (Table VIII) developed hybrid models to simulate concentrations of methotrexate in Lewis lung carcinoma in mice and spontaneous lymphosarcoma in dogs, respectively. These investigators found the transport in tumors to be best modeled by the membrane-limited assumption. Similarly, Weissbrod *et al.* (48) used a hybrid model to calculate the membrane permeability of L-1210 leukemia cells in mice and found these values comparable to *in vitro* values. In contrast, Jain *et al.* (18) used the whole-body model and found the transport of methotrexate in hepatoma 5123 and Walker 256 carcinoma in rats to be flow limited. Jain also estimated the extent of drug metabolism during constant infusion and found the fraction of drug metabolized to be ~20% at the end of a 3-day infusion (49). Further extensions of these models should incorporate synthesis of dihydrofolate reductase in the presence of drug and details of the drug metabolism.

Cisplatin—The antineoplastic activity of cisplatin occurs from its ability to produce intrastrand and interstrand crosslinks in DNA molecules. Cisplatin is known to metabolize by a complex scheme of reactions. The metabolites of the parent compound are considered also to have antineoplastic effects. To this end, parent drug and metabolites represented by one species were modeled with a

Table IX—Model Parameters for Cisplatin in a 10-kg Dog ^a

Tissue	Linear Binding Constant (<i>R</i>)	Other Values	Metabolite	
			Cisplatin	
Muscle	0.7	Kidney clearance (<i>k_k</i>), ml/min	0.5	0.6
Skin	3.5			
Ovaries	1	Bile clearance (<i>k_b</i>), ml/min	0	0.035
Liver	6			
Kidney	8	Metabolism constant, min ⁻¹	0.00416	
GI tract	1			

^a Data taken from Ref. 50.

Table X—Model Parameters for Streptozocin in the Mouse^a

Tissue	Linear Binding Constant (<i>R'</i>)		Mass Transfer Coefficient (<i>h</i>), min ⁻¹		Metabolism Constant (<i>k</i>), min ⁻¹	
	Bioassay	Chemoassay	Bioassay	Chemoassay	Bioassay	Chemoassay
Liver	23.6	19.7	0.0164	0.1392	0.0086	0.0041
Kidney	5.6	7.7	0.0305	0.1625	0.0096	0.0041
Pancreas	—	15.8	—	0.0063	—	0.0041

^a Data (51) reprinted from the *Journal of Pharmaceutical Sciences* with permission; © 1980, American Pharmaceutical Association.

flow-limited scheme containing six compartments in the beagle dog by LeRoy *et al.* (Table IX) (50). Linear binding and first-order metabolism were incorporated using *in vitro* reaction rate constants. The flow-limited model was able to provide an adequate simulation of most of the tissue data. However, disagreement with muscle data, especially at early intervals, might be due to a diffusion limitation.

Streptozocin—Streptozocin is known to inhibit primary DNA synthesis by alkylation of cell components. The drug has a selective toxicity for pancreatic β -cells and is therefore useful in treating pancreatic tumors (*e.g.*, metastatic insulinoma). Weissbrod and Jain have applied a physiologically based hybrid model to describe streptozocin distribution in mice (Table X) (51). This model incorporates three membrane-limited compartments with linear binding and first-order intracellular metabolism. Tissue data obtained by bioassay to determine parent streptozocin and by chemoassay to determine parent streptozocin and its metabolites were compared with simulations. The fit to the parent compound and metabolites was adequate in this work, although the authors suggested that more data were required to describe the transport and metabolism in greater detail.

2-Amino-1,3,4-Thiadiazole—The antineoplastic action of 2-amino-1,3,4-thiadiazole includes inhibition of inosine-5-phosphate dehydrogenase in cells. For this reason, 2-amino-1,3,4-thiadiazole retards the growth of melanomas, lymphosarcomas, and leukemias. A physiologically based pharmacokinetic model was developed by King and Dedrick (Table XI) (52) to describe 2-amino-1,3,4-thiadiazole in the mouse, dog, and monkey. The authors used a flow-limited system with four compartments and represented all metabolites as one species. The rate of metabolism was described as a first-order linear process in mice and as a saturable process in dogs and monkeys. Binding and kidney clearance were considered linear. The authors obtained partition coefficients based on long-term experimental values of serum and tissue concentrations.

The metabolic parameters were obtained by best fit of the model to tissue concentration data. The major excretory pathways were found to be kidney clearance in the mouse and saturable metabolism in the dog and monkey. It seems that because of these interspecies differences, scale-up to humans would be difficult for this substance.

Antibiotics—Antibiotics are prescribed to treat infection. The wide applicability of antibiotics raises questions as to the disposition of these substances in the body. Physiologically based pharmacokinetics provide a tool that can aid in answering these questions.

Cephalosporin Antibiotics—Three cephalosporin antibiotics (cefazolin, cephalexin, and cephadrine) were studied by Greene *et al.* (53) These antibiotics show *in vitro* activity against penicillin-resistant staphylococci and are considered to bind to plasma proteins. The authors compared the simulations using a six-compartmental perfusion model with a classical two-compartmental model, with and without protein binding. Plasma binding, described by the Scatchard equation, was used to fit the models to human plasma data for each cephalosporin administered. The authors obtained good simulations of the plasma data for cefazolin at a 1-g iv dose and for cephalexin at a 0.5-g iv dose, but underpredicted the plasma concentration at times >1.5 hr for cephadrine at a 2-g iv dose. The authors attributed this disagreement to a possible overestimate of the cephadrine clearance value.

β -Lactam Antibiotics— β -Lactam antibiotics include ampicillin, cefazolin, dicloxacillin, methicillin, penicillin G, penicillin V, and others. The uptake, distribution, and elimination of various antibiotics and the model test substance inulin were studied in a 12-compartment model in rats (54). The lung, heart, muscle, skin, gut, and carcass were modeled as cell membrane limited, the liver and kidney as flow limited, and the bone compartment was broken down into bone marrow (flow-limited) and bone cortex (membrane-limited) compartments. Tissue-to-plasma partition coefficients of penicillin V, dicloxacillin, cefazolin, and inulin were determined by *in vivo* experi-

Table XI—Model Parameters for 2-Amino-1,3,4-thiadiazole in the Dog and Monkey^a

Tissue	Linear Binding Constant (<i>R</i>)					
	Mouse		Dog		Monkey	
	Drug	Metabolites	Drug	Metabolites	Drug	Metabolites
Liver	0.9	1.3	0.9	2.8	0.6	1.8
Gut	1.0	1.1	1.0	0.4	0.4	1.3
Kidney	0.9	2.0	1.6	2.0	0.6	3.6
Lean tissue	0.9	0.5	1.0	0.2	0.9	0.3
Kidney clearance (<i>k_k</i>), ml/min						
Drug		0.066		8.8		1.5
Metabolites		0.215		18.3		4.6
Metabolism						
<i>v_{max}</i> , μ g/min		—		19.2		6.3
<i>K_m</i> , μ g/ml		—		0.2		0.5
<i>k</i> , ml/min		0.017		95.0		12.5

^a Data taken from Ref. 52.

Table XII—Model Parameters for Several β -Lactam Antibiotics in the Rat ^a

Tissue	Linear Binding Constant (<i>R</i>)		
	Penicillin V	Dicloxacillin	Cefazolin
Lung	0.157	0.123	0.154
Heart	0.095	0.074	0.101
Muscle	0.062	0.051	0.077
Bone	—	—	0.111
Skin	—	—	0.303
Spleen	0.096	0.088	—
Gut	0.966	1.357	0.114
Liver	0.250	0.430	0.788
Kidney	3.70	1.27	2.79

^a Data taken from Ref. 54.

ments after constant infusion of these substances. Renal and hepatic clearance constants were also determined from independent experiments. Binding to serum proteins (albumin) was considered to be nonlinear for cefazolin and penicillin V, whereas linear binding was used for penicillin G, methicillin, dicloxacillin, and ampicillin (Table XII). Although partition coefficients, binding constants, and elimination parameters were measured for several antibiotics, these authors compared their model to tissue distribution data for cefazolin and inulin only and found good agreement.

Tetracycline—The antibiotic tetracycline is highly active against Gram-positive and Gram-negative organisms. This drug is recommended for treatment of pneumonia, actinomycosis, brucellosis, urinary infections, Rocky Mountain spotted fever, and typhus fever (41). When tetracycline is given to rats during pregnancy, it is known to lead to acute fatty liver syndrome in the mother and teratogenic effects in the fetus. To this end, Olanoff *et al.* developed a physiologically based pharmacokinetic model of tetracycline in nonpregnant (55) and pregnant rats (16) (Table XIII). This model included seven flow-limited compartments in both the maternal section and the fetal section, including a placenta compartment for maternal-to-fetal transfer of the drug. The authors applied linear binding in all compartments and allowed for fetal growth over 21 days. The model was used to determine the controlled release of tetracycline using a trilaminar drug delivery device. The model described the data well and was able to predict the constant tissue concentrations desired of a controlled-release device. The authors had to use uniformly lower values of the partition coefficients in the pregnant rats when compared with the nonpregnant rats. The inclusion of a fetus in such a model represents a significant advance in physiologically based pharmacokinetics.

Table XIII—Model Parameters for Tetracycline in the Pregnant Rat ^a

Tissue	Flow-Limited Linear Binding Constant (<i>R</i>)	
	Maternal	Fetal ^b
Liver	0.97	1.0
Kidney	0.97	1.4
Bone	1.68	4.55
Muscle	1.03	—
GI tract	1.06	1.32
Placenta	—	1.23
Amniotic fluid	—	0.46
Fat	0.7	—

^a Data (16) reprinted from the *Journal of Pharmacokinetics and Biopharmaceutics*; © 1980, Plenum Publishing Corp. ^b Ratio of fetal tissue concentration to maternal plasma concentration at equilibrium.

Anesthetics—Anesthetics are used for temporary suppression of pain, normally during surgery. Based on the knowledge of the uptake, distribution, metabolism, *etc.*, of these substances in the body, physiologically based pharmacokinetics provide an excellent technique to determine dosage regimens to ensure that proper amounts are delivered to the desired region of the body. Biomedical equipment that is used in the delivery of anesthetics can be designed based on pharmacokinetic simulations, thus limiting the danger of experimentation with new equipment.

Halothane—Halothane is a widely used, potent, non-inflammable, and nonexplosive inhalation anesthetic with rapid onset and rapid reversal. Since the pioneering work of Mapleson (56), several flow-limited hybrid models have appeared in the literature to describe the uptake and distribution of halothane in humans (17, 57–59). Since changes in halothane concentration influence cardiac output and distribution, and *vice versa*, many investigations have tried to incorporate this interrelationship in their models. Ashman *et al.* (57) assumed that a uniformly distributed reduction in cardiac output occurred as anesthetic concentration in the viscera increased. After comparing the results of constant and variable cardiac output models, the authors concluded that the differences in these two models were insignificant for the first few minutes, but progressively increased during the first hour to 6%. Zwart *et al.* (17) and Smith *et al.* (58) improved this model by making changes in the cardiac output and its distribution a function of halothane concentration in one or two of the three most important compartments, *i.e.*, brain, myocardium, and arterial blood (Table XIV). The results of this model differed significantly from those models with constant cardiac output and gave new insight into halothane-induced changes in the circulation. Munson *et al.* (59) divided the body into five flow-limited compartments and modeled the effects of reduced ventilation rate and cardiac output on halothane pharmacokinetics. Using this model, these authors were able to predict limits to which

Table XIV—Model Parameters for Halothane in the Human and Lidocaine in the Monkey and Human

Tissue	Flow-Limited Linear Binding Constant (<i>R</i>)	
	Halothane (Human) ^a	Lidocaine (Monkey and Human) ^b
Arterial	2.3	—
Brain		
Grey matter	5.4	1.21
White matter	8.3	
Heart	8.1	—
Well-perfused organs	3.7	—
Poorly perfused organs	5.3	—
Fat (and fatty marrow)	138	2.0
Splanchnic	6.0	—
Muscle	8.1	0.65
Lung	5.3	3.08
Liver	—	0.61
Rapidly equilibrating tissue	—	2.02
Slowly equilibrating tissue	—	0.60
Portal	—	1.53

^a Data (58) reprinted from *Anesthesiology* with permission; © 1972, Lippincott/Harper and Row. ^b Data (65) reprinted from *Clinical Pharmacology and Therapeutics* with permission; © 1974, American Society for Pharmacology and Experimental Therapeutics.

Table XV—Model Parameters for Methohexital, Pentobarbital, and Thiopental in the Human

Parameter	Methohexital ^a	Pentobarbital ^b	Thiopental ^b
Effective fraction			
f_B	$\left(\begin{array}{c} \text{ramp} \\ \text{functions} \\ 0-1.0 \end{array} \right)$	0.985	0.985
f_V		0.963	0.963
f_L		0.980	0.980
f_V		0.200	0.200
Binding sites, $\mu\text{mole/liter}$			
B_1	52 (mg/liter)	5,900	18,400
B_2	870 (mg/liter)	317,000	305,400
Binding equilibrium constant (liter/ μmole)			
k_1	3.3×10^{-2} (liter/mg)	0.2117	0.06
k_2	1.2×10^{-3} (liter/mg)	0.00016	0.000625
Lipid solubility (BA)	65	9.0	100
Michaelis-Menten constants			
K_m , $\mu\text{mole/liter}$	—	4.0	4.0
v_{\max} , $\mu\text{mole/min}$	—	2.63	26.3

^a Data (63) reprinted from the *Journal of Pharmaceutical Sciences* with permission; © 1976, American Pharmaceutical Association. ^b Data (60) reprinted from "Pharmacokinetics in Applications of the Artificial Kidney" with permission; © 1968, Chemical Engineering Progress Symposium Series.

anesthetic drugs and techniques could be used safely.

Hexobarbital, Pentobarbital, Phenobarbital, and Thiopental—These four drugs are the most common barbiturates used in medicine. Thiopental, a local anesthetic used in dental patients, has biological effects similar to methohexital. Hexobarbital and thiopental are short- and ultrashort-acting anesthetics, respectively. This rapidity results from metabolic degradation and physical redistribution. Phenobarbital has a slower rate of action on the brain compared with hexobarbital and thiopental. Pentobarbital is a fast-acting sedative useful in the treatment of insomnia, nausea, etc. The drug is also useful in controlling convulsions such as those which occur in eclampsia, epilepsy, tetany, and strychnine poisoning. Overdoses of barbiturates can lead to death by respiratory failure (41).

To this end, Bischoff and Dedrick (60, 61) developed a four-compartment model (blood, viscera, lean tissue, and adipose tissue) to describe the pharmacokinetics of barbiturates in dogs and humans. By incorporating parameters characterizing lipid solubility, protein binding, and metabolism of thiopental, these authors were able to simulate the tissue data in dogs and plasma data in humans. These authors later applied the thiopental model to pentobarbital which has a lower lipid solubility, less

protein binding, and is metabolized at about one-tenth the rate of thiopental (60). By including these changes, a suicidal dose in the human (43 mg/kg) was simulated (Table XV). These authors also simulated the effect of treatment with an artificial kidney, and using this model, were able to predict the well-known rebound effect in blood, lean tissue, and viscera.

Since Bischoff and Dedrick combined brain, heart, kidneys, liver, etc. as a viscera component, their model can not predict thiopental concentrations in the brain, which is valuable information for optimal therapy. To this end, Chen and Andrade (62) developed a seven-compartment model to predict thiopental kinetics in the brain, plasma, liver, GI tract, lean tissue, adipose tissue, and viscera and obtained good agreement with the data obtained in dogs. A detailed sensitivity analysis indicated the values for fractions of bound drug in various tissues were more sensitive parameters than the others in the model and, therefore, must be determined precisely. Similar to methohexital, the four-compartment model of Bischoff and Dedrick was also extended by Gillis *et al.* (63) to account for the slow approach to equilibrium in human tissues.

The most comprehensive model of barbiturates (hexobarbital, phenobarbital, and thiopental) has been developed recently by Igari *et al.* (Table XVI) (64a). These authors have developed an 11-compartment model which includes lung, venous and arterial plasma, liver, brain, heart, GI tract, kidney, muscle, skin, and adipose tissue. Except for the brain, all tissues were assumed to be flow limited. Partition coefficients, Michaelis-Menten constants for drug metabolism, and binding constants were determined *in vitro* and compared with *in vivo* data. The *in vitro* partition coefficients did not lead to good agreement with the plasma and brain data. When partition coefficients obtained from *in vivo* experiments were used instead, the authors were able to describe the data well. [In a later publication, these authors use a similar model to predict ethenzamide (ethoxybenzamide) concentrations in nine compartments in rats, scaled-up to rabbits (64b), from K_p (partition coefficient) values obtained *via* intravenous bolus injection, constant-rate infusion, and *in vitro* determinations (64c).]

Lidocaine—Lidocaine is a potent anesthetic agent used for infiltration and block anesthesia. It is also used topically for anesthesia of accessible mucous membranes. The action of lidocaine on nerves is considered similar to that of procaine (41). Congestive heart failure patients, when given standard intravenous doses of lidocaine, show ele-

Table XVI—*In Vitro* and *In Vivo* Model Parameters for Hexobarbital, Phenobarbital, and Thiopental^a

Tissue	Thiopental		Hexobarbital		Phenobarbital	
	<i>In Vitro</i>	<i>In Vivo</i>	<i>In Vitro</i>	<i>In Vivo</i>	<i>In Vitro</i>	<i>In Vivo</i>
Lung	2.71	1.16	1.49	3.26	1.14	0.816
Heart	1.91	1.07	1.86	1.12	1.93	0.97
Liver	2.10	5.28	1.45	5.96	1.87	1.92
GI tract	2.02	1.18	1.91	1.26	1.75	1.66
Kidney	2.50	1.18	2.31	1.51	2.03	0.78
Muscle	2.32	0.664	1.34	0.625	1.60	1.05
Skin	3.42	1.94	0.984	0.909	1.88	1.28
Adipose tissue	11.3	2.86	4.13	1.64	0.926	0.318
Liver kinetics						
K_m , $M \times 10^{-3}$		0.103		1.32		—
v_{\max} , $\mu\text{mole/min}/0.25 \text{ kg}$		0.099		8.48		—

^a Data (64a) reprinted from the *Journal of Pharmacokinetics and Biopharmaceutics* with permission; © 1982, Plenum Publishing Corp.

vated blood levels presumably due to decreased circulation and clearance. A physiologically based pharmacokinetic model can be useful in predicting the lidocaine levels of patients suffering from cardiovascular diseases. An eight-compartment flow-limited model to describe the pharmacokinetics of lidocaine in humans and monkeys was developed by Benowitz *et al.* (Table XIV) (65). The authors assumed equilibrium was obtained after 24 hr to obtain experimental tissue-to-plasma partition coefficients in rhesus monkeys. The model was then scaled-up to humans with the same binding parameters as found in the rhesus monkey. Good agreement was found between human plasma data and model predictions. In a later study by Benowitz *et al.* (66), the effects of hemorrhagic shock and sympathomimetic drugs (isoproterenol and norepinephrine) on lidocaine kinetics and regional blood flow in the rhesus monkey were examined. The results obtained have many interesting clinical implications.

Methohexital—Methohexital is a local anesthetic used primarily in dental surgery. Dosage requirements can change from alterations in body distribution processes. Alterations can result from dehydration, uremia, peripheral circulatory failure, increased cardiac output, electrolyte disturbances, hepatic failure, and chronic renal failure.

Using the approach developed by Bischoff and Dedrick for thiopental pharmacokinetics, Gillis *et al.* (63) developed a flow-limited model to describe the distribution of methohexital in the human. Similar to the model of Bischoff and Dedrick, it included details of protein binding and liver metabolism (Table XV). Unlike that of Bischoff and Dedrick, this model used a ramp function to describe the approach to equilibrium in tissue, with characteristic times determined by the perfusion rates. The model described the available data adequately and was used to predict the influence of body alterations (*e.g.*, obesity) on drug distribution.

Procaine—Procaine² is a local anesthetic used primarily in dental surgery. The drug blocks the function of the nerves near an injection site by attaching to and preventing sodium transfer across the nerve cell membrane, thus hindering the formation and propagation of the action potential on the membrane. The process is reversible, so the effects on the cell are only temporary (19). A nine-compartment flow-limited model was developed by Smith *et al.* (67) to describe procaine pharmacokinetics in humans. Independently determined nonlinear binding and nonlinear metabolism terms were incorporated into the model. Model simulations showed good agreement with human data in the arterial plasma, brain, muscle, adipose tissue, and viscera regions. The model was also applied to lidocaine in humans and compared well with the human plasma data.

Trace Metals and Other Ions—Trace metals and other ions are studied for various reasons. Certain endogenous metals and ions are essential for body growth, development, and many daily functions. Several exogenous metals and ions are also required nutritionally by the body (*e.g.*, iodine, chromium) and must be taken in the diet. Other exogenous substances can be lethal at high doses (*e.g.*, cadmium, lithium). To this end, physiologically based

Table XVII—Model Parameters for Bromide in the Rat and Human^a

Tissue	Flow-Limited Linear Binding Constant (<i>R</i>)	Membrane-Limited Linear Binding Constant (<i>R'</i>)	Mass Transfer Coefficient (<i>h</i>), ml/min
Skin	—	0.35	0.015
Kidney	—	0.21	0.0004
Liver	—	0.085	0.0009
Muscle	0.150	—	—
Spleen	0.240	—	—
GI tract	—	0.37	0.0058
Brain	—	0.14	0.00073
Lung	0.376	—	—
Thyroid	0.480	—	—
Heart	0.150	—	—
Adipose tissue	—	0.22	0.0002
Red blood cell compartments			
1	0.30	—	5.0
2	2.79	—	0.019
Residual carcass	0.08	—	—

^a Data (69) reprinted from the *American Journal of Physiology* with permission; © 1978, The American Physiology Society.

pharmacokinetic models can be used to determine proper dietary intake, to predict maximum dosages to ensure against toxicity in high-accumulation or target organs, and also to develop detoxification strategies.

Bromide—Bromide is an essential element for the body. Small amounts are found in table salt and several vegetables. Natural intake of bromide occurs primarily by GI absorption from these sources. Bromide passes through the various body fluids, penetrates red blood cell membranes, and is eliminated *via* the kidneys. Bromide also displaces chloride in extracellular fluid, which may lead to a sedative effect on nerve tissue (68). In this manner, bromide can be used as a tracer to measure the volume of extracellular water (69). The model by Pierson *et al.* (69) applied physiologically based pharmacokinetics to predict the distribution of bromide in rats and then scaled-up to humans (Table XVII). Twelve compartments were included in this model; the muscle, lung, heart, spleen, thyroid, and body compartments were assumed to be flow limited and the skin, adipose tissue, kidney, brain, liver, GI tract, and red blood cell compartments were assumed to be membrane limited. The authors computed the linear binding parameters from steady-state bromide distribution data. The rat model predictions of extracellular volume were compared with known values along with the concentration data. The authors found adequate agreement within the inherent statistical limitations of the data. Identical thermodynamic and transport parameters were used in the scaled-up model and led to good agreement with plasma, skin, muscle, and adipose tissue data in humans. This model and these experiments indicated that bromide was an imperfect tracer for extracellular water because of consistent overprediction of the extravascular water volume.

Cadmium—Cadmium, an exogenous substance, is toxic when present at high levels. Because of this toxicity, cadmium is of primary concern to the metals industry for environmental reasons. Low cadmium doses are found to result in hypertension (70). Accumulation of cadmium in

² Novocain; Breon Laboratories, Inc., New York, N.Y.

Table XVIII—Model Parameters for Cadmium in the Mouse ^a

Tissue	Flow-Limited Linear Binding Constant (R)	Membrane-Limited Linear Binding Constant (R')	Mass Transfer Coefficient (h), min^{-1}
Spleen	0.55	—	—
GI tract	0.53	—	—
Liver	—	19.0	0.16
Kidney	—	7.0	0.03
Red blood cell	—	0.5	0.002
Carcass	0.34	—	—

^a Data taken from Ref. 73.

the testicles of laboratory animals leads to necrosis of this tissue (71). The similarities and dependence in transport and uptake of cadmium to zinc has led to many comparative studies of these two elements (72). Following intake, cadmium is found to clear rapidly from the plasma, bind to subcellular proteins, and accumulate readily in the liver and kidneys (14). The Gerlowski and Jain model (73) combines both membrane-limited and flow-limited compartments to study cadmium uptake in mice (Table XVIII). Membrane-limited liver and kidney compartment simulations show good agreement with the data, which account for 60% of the initial dose. The fit was not as good in the other compartments, especially in the residual carcass compartment where many organs were lumped into one flow-limited compartment. Further improvements can be made in this model when short-term data become available for various organs.

Chloride—Chloride, an endogenous trace element, is essential for electrolytic, osmotic, and acid balances and other bodily functions. Dietary chloride is obtained in animal foods, absorbed through the GI tract, and excreted primarily through the urinary tract (68). Chloride depletion may be a useful treatment for brain edema (74). Gabelnick *et al.* (74) have developed a three-compartment hybrid model (Fig. 4) representing brain, well-perfused, and poorly perfused compartments to study mass transfer of chloride in cats undergoing hemodialysis. Transfer to the brain was considered to occur by diffusion from the well-perfused compartment, by convection from cerebrospinal fluid (CSF), and by mediated transport from the well-perfused compartment. Brain tissue was assumed to be in equilibrium with the CSF. The mass transfer coefficient from the well-perfused compartment to the brain was estimated to be 0.037 ml/min. The transport rate of chloride into the CSF was found to be a constant (0.55 $\mu\text{eq/ml} \cdot \text{min}$) for 60–120-meq/liter plasma chloride concentrations. This behavior indicated the existence of a “saturated pump” and was modeled as a constant infusion term (2.8 $\mu\text{eq/min}$). The authors noted agreement with the data, except for the brain compartment, which experimentally indicates a steady-state equilibrium concentration, unlike the model predictions. This disagreement may have resulted from a possible change in flow rate of the CSF or mediated transport into the brain during hemodialysis.

Lithium—Lithium, an exogenous substance, is used in the treatment of manic-depressive illness. Problems that arise from dosage levels and schedules of lithium have led to the use of pharmacokinetics in determining proper regimens. A model presented by Ehrlich (75) applies a three-compartment scheme representing plasma and extracellular fluid, red blood cells, and muscle-like cells to

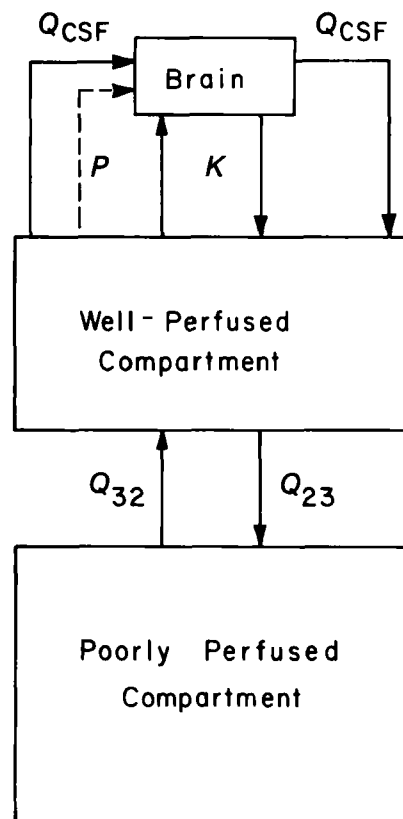


Figure 4—Location of the brain compartment (74). Reprinted from the *Journal of Applied Physiology* with permission; copyright 1980, American Physiological Society.

describe lithium distribution in four human subjects (Table XIX). Linear transport and Michaelis-Menten excretion parameters were incorporated in the hybrid model. The model simulated the data well and suggests that the Li^+ countertransport efflux mechanism of the red blood cell may be shared with the muscle. However, variations in the intercompartment concentrations, because of high concentrations in the liver and kidneys, suggest the need of a larger model consisting of several more compartments when the data become available.

Zinc—Zinc, an endogenous substance, is essential in that DNA and protein syntheses are zinc dependent; also, carbohydrate metabolism, lipid peroxidation, and bone formation require zinc. Deficiencies in zinc may lead to growth retardation and failure of sexual maturation. A comprehensive model (17 tissues, plasma, and red blood cells) was developed to describe zinc distribution in rats (15). In this model, membrane-limited compartments were incorporated with linear binding, transport, and excretion.

Table XIX—Model Parameters for Lithium in the Human ^a

Tissue	Absorption Rate, hr^{-1}
GI tract	
Absorption rate	0.36–1.88
Renal excretion rate	0.09–0.18
Muscle	
Influx	0.26–0.38
Efflux	0.19–0.36
Red blood cells	
Influx	0.12–0.29
Efflux	0.35–0.80

^a Data (75) reprinted from the *Journal of Pharmacokinetics and Biopharmaceutics* with permission; © 1980, Plenum Publishing Corp.

Table XX—Model Parameters for Zinc in the Rat ^a

Tissue	Membrane-Limited	Mass Transfer
	Linear Binding Constant (R')	Coefficient (h), hr ⁻¹
Skin and fur	6.5	0.0339
Muscle	11.0	0.0171
Liver	28.0	0.4076
Intestine	14.8	0.3132
Stomach	18.0	0.1181
Fat	0.7	0.0037
Thyroid	11.3	0.1815
Bone and bone marrow	25.0	0.0799
Heart	13.0	0.1216
Bladder	17.0	0.0739
Prostate	6.0	0.0633
Spleen	15.0	0.2083
Pancreas	20.0	0.1884
Kidney	20.0	0.3278
Brain	11.4	0.0191
Gonads	15.0	0.05
Sex organ	8.0	0.04
Gut lumen	16.0	0.1274
Red blood cell	5.5	0.0376 (ml/hr)
Clearance rate, ml/hr		
Fecal (k _f)	0.14	
Urinary (k _u)	0.15	
Intestinal (k _i)	7.21	
Pancreatic (k _{pan})	2.41	

^a Data (15) reprinted from the *Annals of Biomedical Engineering* with permission; © 1982, Pergamon Press Inc.

The physicochemical parameters were estimated by decomposing this model into hybrid models and minimizing the error between data and model for each tissue (Table XX) (15). Excellent agreement with data was found (average error <10%); however, only a limited number of data were used in estimating the model parameters. A more complete model should incorporate zinc speciation, nonlinear transport and binding, and intercompartmental diffusion.

Environmental Hazards and Toxic Substances—The uptake of many chemicals by the body can lead to harmful effects. Various regulatory agencies impose tolerance levels for hazardous chemicals to ensure safe working conditions. These levels are usually obtained from experiments over short periods of time and formulate an opinion on only one tissue concentration value (e.g., plasma concentration). But, tissue concentrations are known to vary over a wide range throughout the body. Therefore, to ensure that all tissues remain below toxic levels at all times, physiologically based pharmacokinetics may be incorporated into such decision-making processes to set more precise levels.

Acetylacetone—Acetylacetone (2,5-hexanedione) is a neurotoxic metabolite of the industrial solvents *n*-hexane and methyl *n*-butyl ketone. Action of acetylacetone on the sciatic nerves causes axonal damage which characterizes central-peripheral distal axonopathy. Recently, a nine-compartment flow-limited physiologically based pharmacokinetic model was constructed by Angelo and Bischoff (76) to simulate the detailed pharmacokinetics and metabolism in rats (Table XXI). These authors determined equilibrium tissue-plasma distribution ratios based on *in vivo* data determined by constant intravenous infusion of acetylacetone using a surgically implanted infusion pump. Metabolism of acetylacetone was simplified to a three-step series reaction scheme, and the rate constant for the second reaction was considered to be organ specific. Very good agreement with data was found for

Table XXI—Model Parameters for Acetylacetone in the Rat ^a

Tissue	Linear Binding Constant (R)		Tissue-Plasma Turnover Ratio
	Parent Drug	Metabolite	
Liver	1.7	3.4	0.7
Kidney	0.6	3.1	0.75
Lung	0.6	2.5	0.55
Lean tissue	0.4	0.8	1.0
Brain	0.4	0.5	1.4
Sciatic nerve	0.4	0.4	3.0
Spinal cord	0.4	0.5	5.0 (k _{ac} 11.5)
Other values			
Peritoneal permeability, ml/hr			12.0
Linear kidney clearance, ml/hr			
Parent drug			10.0
Metabolite			30.0
First-order metabolism constant, ml/hr			150.0
Carbon-14 incorporation rate constant (plasma), hr ⁻¹			0.03

^a Data (76) reprinted with permission of the author.

single-dose exposures of 0.8 and 8.0 mg/kg ip for the plasma, sciatic nerve, liver, kidney, lung, and lean compartments in the elimination phase; however, the absorption phase was somewhat underpredicted in each case up to 1 hr. Additionally, the spinal cord compartment exhibited a dose-dependent partition coefficient. The model also described the concentrations of metabolites in the plasma, liver, and urine adequately. In multiple dosing (8.0 mg/kg/day ip), simulations reproduced the tissue data well except for plasma data. These data were overpredicted, perhaps due to kinetics of the radioisotope uptake and release by plasma constituents. The early interval behavior suggested the need for a diffusion-limited model with precise blood kinetics.

Chlordecone—Chlordecone³ is a chlorinated organic insecticide which is toxic to most life forms. In industrial sites, workers in contact with chlordecone are found to contract severe cases of tremors. From tests performed on laboratory mice, chlordecone has been found to be a carcinogen. Boylan *et al.* (77) and Bungay *et al.* (78) have shown evidence for bidirectional transport of chlordecone between blood and gut contents in mice. Bungay *et al.* (78) have developed a physiologically based pharmacokinetic model with a detailed enteric transport model to describe the distribution and excretion of a nonadsorbable tracer and parent chlordecone in rats (Table XXII). The GI tract was modeled to include stomach, small intestine, cecum, and large intestine; each organ was represented by a series of well-mixed subcompartments. This model was able to predict the short-term transport kinetics of parent chlordecone as well as substances that are unabsorbed or passively transported across the gut wall. The scaled-up model also provided a rational basis for cholestyramine therapy for victims of chlordecone poisoning.

Nitrate and Nitrite—Nitrosamines, which are known to be potent carcinogens, can be formed endogenously from dietary nitrate. Nitrate enters the body in the diet and also is formed from reduced nitrogen compounds. In addition,

³ Kepone.

Table XXII—Model Parameters for Chlordecone in the Rat^a

Tissue	Membrane-Limited Linear Binding Constant (R)			Mass Transfer Coefficient (h), ml/min		
	Capillary	Mucosa	Lumen	Capillary	Mucosa	Lumen
Stomach	7	1	0.031	0.2	0.002	0.002
Small intestine						
I	8	0.5	0.030	0.3	0.05	0.1
II	7	0.4	0.078	0.26	0.04	0.1
III	6	0.3	0.013	0.25	0.02	0.07
Cecum	5	0.2	0.006	0.09	0.006	0.03
Large intestine	4	0.2	0.005	0.10	0.004	0.02
Fat	15	—	—	—	—	—
Liver	55	—	—	11	—	—
Muscle	5	—	—	—	—	—
Skin	6	—	—	0.54	—	—

^a Data (78) reprinted from the *Journal of Pharmacokinetics and Biopharmaceutics* with permission; © 1981, Plenum Publishing Corp.

the salivary glands transport nitrate from the blood to saliva. By bacterial reaction, nitrate is converted in the oral cavity to nitrite, which is then available to form nitrosamines in the stomach. Therefore, to determine the safe amount of dietary nitrate intake, an understanding of the distribution and metabolic fate of nitrate and nitrite would be useful. To this end, Deen *et al.* (79) developed a physiologically based pharmacokinetic model to simulate nitrate and nitrite concentrations in humans following an oral dose of nitrate (Table XXIII). The model consisted of an oral cavity, stomach, small and large intestines, blood and well-perfused tissues, and lean tissues. Transport between the digestive system, blood pool, and well-perfused tissues was modeled to occur by diffusive and convective means *via* bile, saliva, and gastric and pancreatic juices. The authors were able to simulate data adequately for plasma and salivary nitrate and salivary nitrite. The authors found individual variations in values of the renal clearance constant among groups of subjects. The model was not able to predict in detail the fate of reduced nitrogen, *e.g.*, reabsorption from the GI tract, exhalation of gaseous products, *etc.* Denitrification in the oral cavity is also known to occur, but was not incorporated in this model and needs to be further investigated along with the fate of the nitrite presented to the stomach.

Polychlorinated Biphenyls—Polychlorinated biphenyls

(PCB's) are widely recognized as a highly toxic environmental hazard. These substances appear throughout the food chains of all animals. Highly chlorinated biphenyl molecules are known to persist in the body for long periods of time (10–15 years) and are potent inducers of microsomal enzyme activity. Metabolism of polychlorinated biphenyls occurs primarily in the liver, and the metabolites are known to have carcinogenic effects. Polychlorinated biphenyls are known to accumulate primarily in the adipose tissue. Anderson *et al.* (80) and Lutz *et al.* (81) each applied a six-compartment flow-limited model to describe the disposition and metabolism of polychlorinated biphenyls (1-, 2-, 5-, and 6-chlorinated biphenyls) in rats. These authors concluded that a membrane-limited model may be more appropriate for pharmacokinetics of polychlorinated biphenyls in the skin compartment. The alternative would have been to divide the skin into a number of compartments to model the heterogeneous perfusion rate in the skin. The pharmacokinetics of 3,3',5,5'-tetrachlorobiphenyl (4-chlorinated biphenyl) and its metabolites were also studied in rats by Tuey and Mathews (Table XXIV) (82) using the framework developed by Lutz *et al.* Except for 4-chlorinated biphenyl, the rate of metabolism of four polychlorinated biphenyls (1-, 2-, 5-, and 6-chlorinated biphenyls) decreased as the degree of chlorination increased. The rate of metabolism of 4-chlorinated biphenyl was found to be less than that of 5-chlorinated biphenyl and greater than that of 6-chlorinated biphenyl. However, the relative rates of various polychlorinated biphenyls could be ordered according to the number of adjacent unsubstituted carbon atom pairs they contained. These authors, therefore, suggested that the chlorine po-

Table XXIII—Model Parameters for Nitrite in the Human^a

Tissue	First-Order Rate Constant, hr ⁻¹	Reaction Rate Constant for Nitrate, hr ⁻¹	P/V, hr ⁻¹
Intestinal segment			
1	0.21	0.84	5.1
2	0.21	0.84	5.1
3	0.21	0.84	2.0
4	2.1	8.4	1.1
5	2.1	8.4	1.1
6	2.1	8.4	1.1
Gastric emptying	2.0–9.0	—	—
Liver	0–0.038	—	—
Oral cavity	4.8	0–50	—
G1	0.8	—	—
G2	0	—	—
Other values			
Renal clearance liter/hr		1.6–2.5	
K_m , mM		1.5	
V_{max}/K_m , hr ⁻¹		38	
Fraction of nitrite lost in stomach by reaction		0.4	
R (gastric juice to plasma)		18–28	
R (saliva to plasma)		20	

^a Data (79) reprinted with permission of the authors.

Table XXIV—Model Parameters for 3,3',5,5'-Tetrachlorobiphenyl in the Rat^a

Tissue	Flow-Limited Linear Binding Constant (R)	
	Parent Drug	Metabolite
Liver	6	2
Muscle	1	0.1
Skin	7	0.3
Adipose tissue	220	0.5
Gut lumen	—	1
Others, ml/hr		
Liver metabolism constant (k)		14.7
Kidney clearance (k_k)		0.7
Biliary clearance (k_b)		12.1
Fecal transport		0.05
Gut reabsorption		0.01

^a Data (82) reprinted from *Drug Metabolism and Disposition* with permission; © 1977, American Society for Pharmacology and Experimental Therapeutics.

Table XXV—Model Parameters for Digoxin in the Rat, Dog, and Human

Tissue	Flow-Limited Linear Binding Constant (<i>R</i>)		
	Rat ^a	Dog ^b	Human ^b
Heart	1.6	40	40
Skeletal muscle	1.4	9	9
Skin, fat, etc.	1.0	9	9
Kidney	1.9	200	200
Liver	7.9	15	15
GI tract			
Tissues	30.0	30	30
Contents	—	—	—

^a Data (84) reprinted from the *Journal of Pharmaceutical Sciences* with permission; © 1977, American Pharmaceutical Association. ^b Data (85) reprinted from the *Journal of Pharmaceutical Sciences* with permission; © 1977, American Pharmaceutical Association.

sition is more important than the degree of chlorination.

Other Substances—2-Butanol—Pretreatment with 2-butanol and its metabolites is known to potentiate the hepatotoxicity of carbon tetrachloride. Assuming that the only important site of 2-butanol metabolism is in the liver, a two-compartment model consisting of a volume of distribution compartment and a flow-limited liver compartment was developed for 2-butanol and its metabolites butanone, 3-hydroxy-2-butanone, and 2,3-butanediol by Dietz *et al.* (83). The model included transport to the site of metabolism, inhibition of the transformation of butanone to 3-hydroxy-2-butanone, reabsorption of the latter in the liver, and elimination of all four compounds from the animal. The model adequately described the blood data for each of these species after intravenous injections of 3-hydroxy-2-butanone and 2,3-butanediol and following oral administration of 2,3-butanediol and 2-butanol. These simulations also suggested that a 28–30% molar dose of 2,3-butanediol relative to 2-butanol and butanone gave comparable 2,3-butanediol blood kinetics. These authors suggested that there is need for incorporating saturable transport, both linear and saturable binding, and the interactions of 2-butanol and its metabolites with enzymes and other cellular components when appropriate data become available.

Digoxin—Digoxin is one of the cardiac glycosides used in the treatment of heart diseases. As a cardiotonic, digoxin increases myocardial contraction force, and as a depressant, digoxin decreases cardiac rate. A physiologically based pharmacokinetic study was performed on digoxin and its metabolite by Harrison and Gilbaldi (Table XXV) (84). Eight flow-limited compartments were considered with metabolism in the liver, linear tissue binding, and linear excretion in rats. Good agreement was found with plasma, heart, muscle, and liver tissue data and urinary excretion data following an intravenous dose. The model was then altered to include cholestasis and renal failure by setting biliary secretion and renal clearance rates equal to zero, respectively. Plasma and urinary excretion data from rats with ligated bile ducts or ligated ureters were found to be in good agreement with model simulations. The same model was then modified for dogs and scaled-up to humans (85). The simulations agreed well with urinary excretion data and kidney, heart, liver, and muscle tissue data in the dog. When scaled-up to humans the model underpredicted early interval plasma data, but adequately described the urinary excretion data following a single intravenous dose. This discrepancy in plasma data may be due to differences in binding parameters between dogs and humans, or a

Table XXVI—Model Parameters for Ethanol in the Dog and Rat

Parameter	Dog ^a	Rat ^b
v_{max} , mg/ml-hr	0.1992	11.64
Michaelis constant (K_m), mg/ml	0.0095	0.000041
Distribution rate		
k_{13}	0.0005	—
k_{31}	0.1782	—

^a Data (87) reprinted from the *Journal of Pharmacokinetics and Biopharmaceutics* with permission; © 1981, Plenum Publishing Corp. ^b Data (86) reprinted from *Biochemical Pharmacology* with permission; © 1973, Pergamon Press Inc.

diffusion limitation may exist in this system. Steady-state concentration levels predicted were in the same range as those found postmortem in human plasma, heart, and skeletal muscle; however, liver and kidney concentrations were predicted to be 1.5–2 times and 2–3 times the patient data, respectively. While the model described the plasma data in patients with moderate renal impairment, the model underpredicted the plasma data in anuric patients. This discrepancy may have resulted from an effect on the transport and binding parameters by uremia.

Ethanol—Ethyl alcohol is known to act on the central nervous system causing excitation followed by a depressed state. On ingestion, ethanol is rapidly absorbed from the small intestine and is rapidly metabolized to acetic acid by active acetyl oxidative enzymes in the liver (41). Thus, the primary concern for ethanol in the body from a modeling point of view is in the hepatic system. A two-compartment hybrid model consisting of the liver and the remainder of the body, which were interconnected by the hepatic artery and vein, was developed by Dedrick and Forrester for rats (Table XXVI) (86). The authors concluded that *in vitro* Michaelis–Menten kinetic parameters for the liver alcohol dehydrogenase agreed well with the model parameters; however, a significant artifact may be introduced if the body is considered to be a single compartment. A three-compartment hybrid model was recently developed by Rheingold *et al.* (87) to account for the observed vascular concentration gradients, blood flow limitations, and liver metabolism. These compartments included: the liver; the peripheral circulation represented by the femoral artery, peripheral capillaries, and femoral vein in series; and a deep compartment. The model was fitted to femoral artery and vein data following a 10-min constant infusion of ethanol *via* the cephalic vein at doses of 0.13 and 0.26 g/kg. The values of the metabolism parameters did not agree with those of Dedrick and Forrester.

Phenolsulfonphthalein — Phenolsulfonphthalein (phenol red) is useful as a diagnostic agent to determine the functional activity of the kidney; *i.e.*, intravenous injection of phenolsulfonphthalein has a longer residence time in impaired kidneys (41). A physiologically based pharmacokinetic model was developed in the dogfish shark (*Squalus acanthias*) by Bungay *et al.* (Table XXVII) (88). The dogfish shark was chosen to study physiologically based pharmacokinetics in aquatic animals because of the large amounts of pollutants in the ocean, the scalability of pharmacokinetics to lower species, and the abundance of experimental methodology available in fish. This model consisted of three flow-limited compartments representing the kidney, liver, and muscle, a two-subcompartment bile duct, and a plasma compartment. The linear binding constants for the liver and muscle were obtained from the

Table XXVII—Model Parameters for Phenolsulfonphthalein in the Dogfish Shark^a

Tissue	Flow-Limited Linear Binding Constant (<i>R</i>)	Clearance Constant (<i>k</i>), ml/min·kg
Kidney	8	0.36
Liver	4	0.62
Muscle	0.1	—
Other		
Bile duct subcompartments	retention time (τ), 120 min ($n = 2$)	

^a Data (88) reprinted from the *Journal of Pharmacokinetics and Biopharmaceutics* with permission; © 1976, Plenum Publishing Corp.

equilibrium data; the kidney constants were determined by trial and error. Clearance constants were determined from experimental data. Although agreement between the model and data was good, the concentrations predicted in the liver and kidneys were lower than the measured values during the distribution phase, while plasma predictions were higher than data at early intervals. This discrepancy indicates the possibility of higher plasma flow rates than reported in the literature. The agreement between predictions and urine data was good over the entire 48 hr following injection; however, the bile data were lower than the predicted values at 24 and 48 hr. Incorporation of enterohepatic circulation might reduce this discrepancy, as suggested by these authors.

Salicylates—Salicylates have been found to produce marked antipyretic and analgesic effects, and are used to treat rheumatic fever and rheumatic tonsillitis. These substances are easily absorbed from the upper GI tract and spread readily through the tissues. Seventy to eighty percent is usually excreted through the kidneys as free acid (41). A seven-compartment flow-limited model was applied to study the pharmacokinetics of salicylates in the plasma, brain, liver, GI tract, muscle, visceral region, and adipose tissue of dogs by Chen *et al.* (Table XXVIII) (89). The CSF concentration of salicylates was determined by mass balance around the brain, CSF, and blood. Three markedly different dosages, from therapeutic to severely intoxicating levels, were given to determine the appropriateness of dosage regimens. The model was able to predict the data extremely well over all dosages. In addition, comparison of the model with dogs treated with hemoperfusion to remove salicylates was presented. In all cases the predicted concentrations agreed well with the data.

Sulfobromophthalein and Warfarin—Sulfobromophthalein dramatically decreases the elimination of warfarin, an anticoagulant, in the bile. The kinetics of this effect are well known and concentration of both drugs can

Table XXVIII—Model Parameters for Salicylates in the Dog^a

Tissue	Ratio of Blood Volume in Organ Capillaries to Total Blood Volume (<i>R</i>)
Blood pool	0.46
Brain	0.007
Liver	0.087
Viscera	0.091
GI tract	0.163
Muscle	0.164
Adipose tissue	0.028

^a Data (89) reprinted from the *Journal of Pharmaceutical Sciences* with permission; © 1978, American Pharmaceutical Association.

Table XXIX—Model Parameters for Sulfobromophthalein and Warfarin in the Rat^a

Tissue	Flow-Limited Linear Binding Constant (<i>R</i>)	
	Sulfobromophthalein	Warfarin
Muscle	0.10	0.060
Kidney	1.20	0.48
Liver	2456	1.08
Elimination constants		
Primary		
v_{\max} , 10 ⁻⁹ mole/min·ml (liver)	23.6	0.051
K_m , 10 ⁻⁹ mole/ml	174.0	65.0
Secondary		
v_{\max}	15.0	—
K_m	64.1	—

^a Data (91) reprinted from the *Journal of Pharmacokinetics and Biopharmaceutics* with permission; © 1979, Plenum Publishing Corp.

be easily measured (41). These properties make sulfobromophthalein a useful agent for a physiologically based pharmacokinetic study. Montandon *et al.* (90) have developed a model to describe total sulfobromophthalein (unchanged plus conjugated) in the hepatic system of rats and have scaled it to humans (Table XXIX). Two flow-limited compartments for liver and extrahepatic tissue with linear binding, a three-subcompartment bile duct, and a plasma compartment were incorporated. The model simulations compared well with data from the bile, liver, and plasma following a 200-nmoles/min/kg iv infusion in rats. The scaled-up model also agreed with human plasma data following a constant intravenous infusion with or without a rapid intravenous priming dose. The relative inaccuracy between the model and data for the first 10 min following rapid intravenous injection may be corrected by including different kinetics of conjugated and unconjugated sulfobromophthalein in the model. A recent rat model by Luecke and Wosilait (91) improved the aforementioned model by replacing the extrahepatic compartment with the kidney compartment and using the Michaelis–Menten equations for enzymatic processes involved in the drug elimination *via* two pathways (Table XXIX). The model described the plasma and bile data of warfarin and sulfobromophthalein following a 1-mg/kg iv dose of warfarin at time zero and a 50-mg/kg dose of sulfobromophthalein at 60 min. This model provides a framework to study drug interaction using single-drug models.

Tetraethylammonium chloride—The tetraethylammonium cation is effective in blocking vasomotor impulses to blood vessels, thus producing reduction of gastric acidity, GI motility, and partial or complete block of impulses to structures innervated by the autonomic nervous system such as the eye, sweat gland, and bladder (41). An eight-compartment model was developed to describe transport of the tetraethylammonium ion in the rat by Mintun *et al.* (Table XXX) (92). In the development of the model the authors first assumed a flow limitation. However, the data showed no steady-state concentration of tetraethylammonium ion, which the model predicted should occur after a few hours. The authors then incorporated a passive-diffusion membrane limitation. This type of model was not able to predict either the early interval peak or the late interval high concentration associated with the data. On the other hand, the authors were able to predict the data well by incorporating both passive

Table XXX—Model Parameters for Tetraethylammonium Chloride in the Rat ^a

Tissue	Half Saturation Concentration for Transport (K_m), $\mu\text{g/ml}$	Maximum Transport Velocity (v_{max}), $\mu\text{g/min}$	Permeability (k_i), ml/min
Liver	3.0	75.0	2.0
Kidney	1.0	60.0	0.8
Gut	2.0	9.0	0.3
Lung	0.3	0.5	0.05
Heart	0.065	0.32	0.03
Carcass			
rapid	—	—	400
slow	—	—	0.5

^a Data (92) reprinted from the *Journal of Pharmacokinetics and Biopharmaceutics* with permission; © 1980, Plenum Publishing Corp.

and saturable transport across the capillary membrane. Since *in vitro* estimates of drug transport and permeability parameters led to poor agreement with the *in vivo* data, these parameters were fitted with a semiempirical curve-fitting technique. Although the model led to an adequate representation of the intravenous data, these authors questioned the assumption of unidirectional active transport in their model. The incorporation of bidirectional transport and the division of the carcass compartment into subcompartments representing various tissues were improvements suggested by these authors.

CONCLUSIONS

The objective of this review article was to present a unified theoretical framework for physiologically based pharmacokinetics. To this end, historical and technical developments in this area of research were discussed briefly. The comparison between experimental and theoretical results on the distribution of over 37 agents in various mammals were summarized according to their applications. Several important and poorly understood problems were pointed out at various places in the text in the hope of stimulating interest in the investigations involved in this area of research.

Some important problems that deserve further attention are:

1. While simplified models of various organs (*e.g.*, lungs, heart, brain, enterohepatic system, kidneys) appear to give adequate results in several applications, a more complete anatomical description is needed. In reality, lungs receive the cardiac output *via* the pulmonary circulation for oxygenation and a small amount *via* the bronchial circulation for the lung tissue. In most analyses, however, the lung component is placed in series with a single plasma compartment (Fig. 5A) (29, 31). In a limited number of analyses the plasma compartment is divided into the arterial and venous pools with the lung placed between them, consistent with the anatomy (54, 64). A more complete model would include the bronchial circulation as well (Fig. 5B). Similarly, a complete model of the heart would include both the coronary and cardiac flows. Detailed models of the kidneys (93), brain, eyes (94–96), and enterohepatic system (43, 78), which have been discussed elsewhere, should be of help in developing more comprehensive physiologically based pharmacokinetic models (Figs. 1 and 3).

2. The modeling of the uptake of a substance that binds to the red blood cells presents anatomical queries,

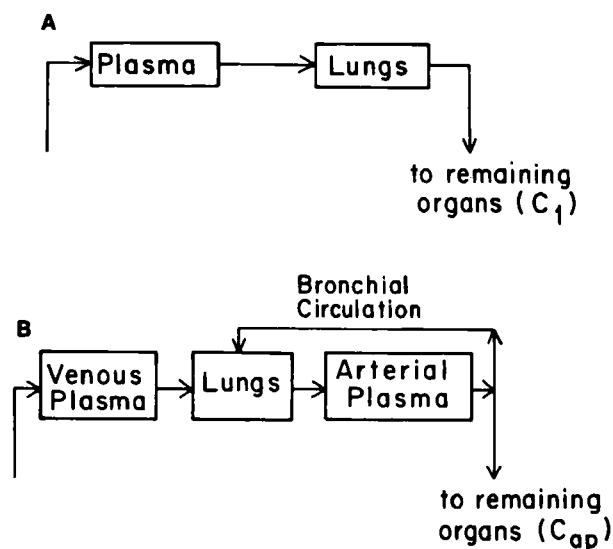


Figure 5—Physiological location of the lung compartment with (A) only one plasma compartment and no bronchial circulation and (B) two plasma compartments with bronchial circulation.

since red blood cells are present in every tissue throughout the body. As shown in Fig. 1, the red blood cells are lumped into one compartment and connected to the plasma compartment where transport is considered to occur, normally by diffusion. A first-order approximation is made by assuming that the transfer of the substance occurs only from the plasma compartment and that the red blood cells occupy dead space for transfer. This method is able to describe the data well, but a detailed model should account for the presence of erythrocytes in each tissue.

3. Although the assumption of no intercompartmental transfer by diffusion is valid for major organs such as the liver, kidneys, heart, *etc.*, the assumption does not realistically apply to poorly perfused organs and tissues. The bone, muscle, and fat organs are usually considered to be separate components with no diffusional transfer; however, this may not be the case for some agents. A first-order approximation to alleviate this limitation would be to assume diffusional mass transfer across these compartments. To date no physiologically based model has used or required this approach to describe data.

4. For many tissues, *e.g.*, solid tumors, the intratissue concentration gradients can be large and each compartment or subcompartment may not behave as a well-mixed phase (97). When this is the case, the lumped-compartment approach applied to date in physiologically based pharmacokinetic modeling may not be applicable, and a distributed parameter approach may be preferred to describe spatial concentration profiles in various tissues (97–101). However, detailed descriptions of convective and diffusive mass transfer in tissues are mathematically intractable. The boundary conditions, due to the complex geometries of the tissue, may also be difficult. Finally, the solution of the partial differential equations may require an enormous amount of computer time. To achieve this end, finite difference or finite element numerical techniques could alleviate some of these problems.

5. Effect of the disease state can significantly alter the pharmacokinetics of an agent by changing its transport, excretion, or metabolism. As discussed in this review article, some models have been able to simulate the effects

of renal and/or hepatic impairment and hemodialysis in uremic patients.

6. Use of multiple drugs is common for the treatment of various diseases, e.g., combination chemotherapy for cancer. Interaction of various drugs can lead to significant alterations in the excretion kinetics if they share the same biochemical mechanism (91). Models for drug interaction need to be developed on the basis of single-drug models.

7. A novel application for physiologically based pharmacokinetics would be in cancer treatment when chemotherapy is used in conjunction with other methods of cancer therapy, e.g., radiation, hyperthermia, immunotherapy, and surgery. In multimodal therapy, both the physicochemical (e.g., mass transfer coefficient and binding constants) and the physiological parameters (e.g., tissue volume and perfusion rates) may change. The effects of temperature on the physiological properties have been studied, but such information has not been incorporated in physiologically based pharmacokinetic models to date (101, 102).

8. Use of certain agents may lead to changes in the cell-cycle parameters involved with enzyme synthesis, drug resistance, or cell death (103). Incorporation of cytokinetics and detailed biochemical processes in physiologically based models remains a challenging problem with useful applications.

9. Although sophisticated numerical techniques are available for parameter estimation, most investigators have estimated the physicochemical parameters not measured independently by "eye-balling." One reason for this procedure is, perhaps, that the estimation of a large number of parameters is expensive. The problem can, however, be alleviated by dividing the whole body into a number of hybrid models, and estimating parameters for each tissue by using plasma as the forcing function. Such a sequential optimization approach has been successfully applied for zinc and pentostatin pharmacokinetics (15, 39).

10. While the ultimate goal of physiologically based pharmacokinetics is to scale-up small animal data to humans and to develop rational clinical protocols, such applications have been limited (37). Perhaps the paucity of human data and the large amount of information needed to develop these models prohibit their use in the clinical situation. Utilization of hybrid models, however, offers an attractive alternative to both classical and physiological approaches (40). Unless this approach is widely applied in clinical situations, its full potential will not be realized.

APPENDIX: GLOSSARY

- a = maximum facilitated transport rate (mole/min)
 a' = strong-binding constant (mole/ml)
 b = Michaelis constant for saturable transport (mole/min)
 C = tissue concentration (mole/ml)
 ϵ = dissociation constant (mole/ml)
 $g(t)$ = injection function (mole/min)
 h = mass transfer coefficient (ml/min)
 k = first-order kinetic rate constant (ml/min)
 K_c = elimination saturation concentration (mole/ml)

- K_m = Michaelis metabolism saturation constant (mole/ml)
 n = flux across capillary or cell membrane (mole/min)
 R = flow-limited linear binding constant (dimensionless)
 $r_i(t)$ = rate of drug disappearance by metabolism in compartment i (mole/min)
 R' = membrane-limited linear binding constant (dimensionless)
 Q = tissue plasma flow rate (ml/min)
 q = excretion rate (mole/min)
 t = time (min)
 V = tissue volume (ml)
 v_{\max} = maximum reaction velocity (mole/min)

subscripts

- i = i th organ (compartment)
 p = plasma compartment

superscripts

- C = cellular compartment
 E = extracellular compartment
 I = interstitial compartment
 V = vascular compartment
 $*$ = free drug

REFERENCES

- (1) K. B. Bischoff, *Cancer Chemother. Rep.*, **59**, 777 (1975).
- (2) K. J. Himmelstein and R. J. Lutz, *J. Pharmacokinet. Biopharm.*, **7**, 127 (1979).
- (3) H.-S. G. Chen and J.F. Gross, *Cancer Chemother. Pharmacol.*, **2**, 85 (1979).
- (4) J. G. Wagner, "Biopharmaceutics and Relevant Pharmacokinetics," Drug Intelligence Publications, Hamilton, Ill. 1971.
- (5) J. G. Wagner, "Fundamentals of Clinical Pharmacokinetics," Drug Intelligence Publications, Hamilton, Ill. 1975.
- (6) L. Sharney, L. R. Wasserman, and N. R. Geritz, *Am. J. Med. Electron.*, **3**, 249 (1964).
- (7) S. Riegelman, J. Loo, and M. Rowland, *J. Pharm. Sci.*, **57**, 117 (1968).
- (8) K. Schmidt-Nielsen, *Fed. Proc. Fed. Am. Soc. Exp. Biol.*, **29**, 1524 (1970).
- (9) R. L. Dedrick, *J. Pharmacokinet. Biopharm.*, **1**, 435 (1973).
- (10) T. Teorell, *Arch. Intern. Pharmacodyn.*, **57**, 205 (1937).
- (11) R. Bellman, J. A. Jaquez, and R. Kabala, *Bull. Math. Biophys.*, **22**, 181 (1960).
- (12) K. B. Bischoff and R. G. Brown, *Chem. Eng. Prog. Symp. Ser.*, **62**, 33 (1966).
- (13) D. J. Cutler, *J. Theor. Biol.*, **73**, 329 (1978).
- (14) L. Friberg, M. Piscator, G. F. Nordberg, and T. Kjellstrom, "Cadmium in the Environment," Cleveland Rubber Co., Cleveland, Ohio, 1974.
- (15) R. K. Jain, L. E. Gerlowski, J. M. Weissbrod, J. Wang, and R. N. Pierson Jr., *Ann. Biomed. Eng.*, **9**, 347 (1982).
- (16) L. S. Olanoff and J. M. Anderson, *J. Pharmacokinet. Biopharm.*, **8**, 599 (1980).
- (17) A. Zwart, N. T. Smith, and J. E. W. Beneken, *Comput. Biomed. Res.*, **5**, 228 (1972).
- (18) R. K. Jain, J. Wei, and P. M. Gullino, *J. Pharmacokinet. Biopharm.*, **7**, 181 (1979).
- (19) E. E. Selkurt, "Basic Physiology for the Health Sciences," Little, Brown and Co., Boston, Mass. 1975.
- (20) W. D. Stein, "The Movement of Molecules Across Cell Membranes," Academic, New York, N.Y., 1967.
- (21) E. N. Lightfoot, "Transport Phenomena and Living Systems—Biomedical Aspects of Momentum and Mass Transport," Wiley, New York, N.Y., 1974.
- (22) A. Goldstein, L. Aronow, and S. M. Kalman, "Principles of Drug Action," Harper and Row, New York, N.Y., 1969.
- (23) E. M. Ariens (Ed.), in "Molecular Pharmacology," Academic, New York, N.Y., 1964.

- (24) K. J. Himmelstein and J. F. Gross, *J. Pharm. Sci.*, **66**, 1441 (1977).
- (25) R. L. Dedrick, D. S. Zaharko, and R. J. Lutz, *J. Pharm. Sci.*, **62**, 882 (1973).
- (26) R. F. Brown, *Trans. Biomed. Eng.*, **27**, 1 (1980).
- (27) Y. Bard, "Nonlinear Parameter Estimation," Academic, New York, N.Y., 1974.
- (28) B. Carnahan, H. A. Luther, and J. O. Wilkes, "Applied Numerical Methods," Wiley, New York, N.Y., 1969.
- (29) R. J. Lutz, W. M. Galbraith, R. L. Dedrick, R. Shrager, and L. B. Mellett, *J. Pharmacol. Exp. Ther.*, **200**, 469 (1977).
- (30) T. R. Tritton and G. Yee, *Science*, **217** (July), 248 (1982).
- (31) P. A. Harris and J. F. Gross, *Cancer Chemother., Rep.*, **59**, 819 (1975).
- (32) K. K. Chan, J. L. Cohen, J. F. Gross, K. J. Himmelstein, J. R. Bateman, Y. Tsu-Lee, and A. S. Marlis, *Cancer Treatment Rep.*, **62**, 1161 (1978).
- (33) J. G. Townsend, "Physiologically Based Pharmacokinetics of Anti-Cancer Drugs and Toxic Substances—Applications to Adriamycin and Ethylene Glycol," Master's Thesis, Carnegie-Mellon University, April 1980.
- (34) L. E. Gerlowski, "Physiologically Based Pharmacokinetics of Anti-Cancer Agents and Trace Metals—Adriamycin, Zinc, and Cadmium," Master's Thesis, Carnegie-Mellon University, May 1982.
- (35) R. L. Dedrick, D. D. Forrester, and D. H. W. Ho, *Biochem. Pharmacol.*, **21**, 1 (1972).
- (36) R. L. Dedrick, D. D. Forrester, J. N. Cannon, S. M. El Dareer, and L. B. Mellett, *Biochem. Pharmacol.*, **22**, 2405 (1973).
- (37) R. L. Dedrick, C. E. Meyers, P. M. Bungay, and V. T. DeVita, Jr., *Cancer Treatment Rep.*, **62**, 1 (1978).
- (38) P. F. Morrison, T. L. Lincoln, and J. Aroesty, *Cancer Chemother. Rep.*, **59**, 861 (1975).
- (39) F. G. King and R. L. Dedrick, *J. Pharmacokinet. Biopharm.*, **9**, 519 (1981).
- (40) J. M. Collins, R. L. Dedrick, F. G. King, J. L. Speyer, and C. E. Meyers, *Clin. Pharmacol. Ther.*, **28**, 235 (1980).
- (41) G. L. Jenkins, W. H. Hartung, K. E. Hamlin, and J. B. Data, "The Chemistry of Organic Medicinal Products," Wiley, New York, N.Y., 1975.
- (42) L. Tterlikkis, E. Ortega, R. Solomon, and J. L. Day, *J. Pharm. Sci.*, **66**, 1454 (1977).
- (43) K. B. Bischoff, R. L. Dedrick, and D. S. Zaharko, *J. Pharm. Sci.*, **59**, 149 (1970).
- (44) K. B. Bischoff, R. L. Dedrick, D. S. Zaharko, and J. A. Longstreth, *J. Pharm. Sci.*, **60**, 1128 (1971).
- (45) D. S. Zaharko, R. L. Dedrick, and V. T. Oliverio, *Comp. Biochem. Physiol.*, **42A**, 183 (1972).
- (46) D. S. Zaharko, R. L. Dedrick, A. L. Peal, J. C. Drake, and R. J. Lutz, *J. Pharmacol. Exp. Ther.*, **189**, 585 (1974).
- (47) R. J. Lutz, R. L. Dedrick, J. A. Straw, M. M. Hart, P. Klubes, and D. S. Zaharko, *J. Pharmacokinet. Biopharm.*, **3**, 77 (1975).
- (48) J. M. Weissbrod, R. K. Jain, and F. M. Sirotnak, *J. Pharmacokinet. Biopharm.*, **6**, 487 (1978).
- (49) R. K. Jain, "Dynamics of Drug Distribution in Solid Tumors," PhD Dissertation, University of Delaware, 1976.
- (50) A. F. LeRoy, R. J. Lutz, R. L. Dedrick, C. L. Litterst, and A. M. Guarino, *Cancer Treatment Rep.*, **63**, 59 (1979).
- (51) J. M. Weissbrod, and R. K. Jain, *J. Pharm. Sci.*, **69**, 691 (1980).
- (52) F. G. King, R. L. Dedrick, *Cancer Treatment Rep.*, **63**, 1939 (1979).
- (53) D. S. Greene, R. Quintiliani, and C. H. Nightingale, *J. Pharm. Sci.*, **67**, 191 (1978).
- (54) A. Tsuji, T. Yoshikawa, K. Nishide, H. Minami, M. Kimura, E. Nakashima, T. Terasaki, E. Miamoto, C. H. Nightingale, and T. Yamana, *J. Pharm. Sci.* (In Press).
- (55) L. Olanoff, T. Koinis, and J. M. Anderson, *J. Pharm. Sci.*, **68**, 1151 (1979).
- (56) W. W. Mapleson, *J. Appl. Physiol.*, **18**, 197 (1963).
- (57) M. N. Ashman, W. B. Blesser, and R. M. Epstein, *Anesthesiology*, **33**, 419 (1970).
- (58) N. T. Smith, A. Zwart, and J. E. W. Beneken, *Anesthesiology*, **37**, 47 (1972).
- (59) E. S. Munson, E. I. Eger, and D. L. Bowers, *Anesthesiology*, **38**, 251 (1973).
- (60) R. L. Dedrick, and K. B. Bischoff, *Chem. Eng. Prog. Sym. Ser.*, **64**, 32 (1968).
- (61) K. B. Bischoff and R. L. Dedrick, *J. Pharm. Sci.*, **57**, 1346 (1968).
- (62) C. N. Chen, and J. D. Andrade, *J. Pharm. Sci.*, **65**, 717 (1976).
- (63) P. P. Gillis, R. J. DeAngelis, and R. L. Wynn, *J. Pharm. Sci.*, **65**, 1001 (1976).
- (64) (a) Y. Igari, Y. Sugiyama, S. Awazu, and M. Hanaro, *J. Pharmacokinet. Biopharm.*, **10**, 53 (1982). (b) J. H. Lin, Y. Sugiyama, S. Awazu, and M. Hanaro, *J. Pharmacokinet. Biopharm.*, **10**, 649 (1982). (c) J. H. Lin, S. Awazu, and M. Hanaro, *J. Pharmacokinet. Biopharm.*, **10**, 637 (1982).
- (65) N. Benowitz, R. P. Forsyth, K. L. Melmon, and M. Rowland, *Clin. Pharmacol. Ther.*, **16**, 87 (1974).
- (66) N. Benowitz, R. P. Forsyth, K. L. Melmon, and M. Rowland, *Clin. Pharmacol. Ther.*, **16**, 99 (1974).
- (67) R. H. Smith, D. H. Hunt, A. B. Seifen, A. Ferrari, and D. S. Thompson, *J. Pharm. Sci.*, **68**, 1016 (1979).
- (68) J. M. Orten and O. W. Neuhaus, "Biochemistry," C. V. Mosby, St. Louis, Mo., 1970.
- (69) R. N. Pierson, Jr., D. C. Price, J. Wang, and R. K. Jain, *Am. J. Physiol.*, **235**, F254 (1978).
- (70) G. F. Nordberg, *Environ. Physiol. Biochem.*, **1**, 171 (1971).
- (71) H. A. Schroeder and W. H. Vinton, Jr., *Am. J. Physiol.*, **202**, 315 (1962).
- (72) B. S. Kingsley and J. M. Frazier, *Am. J. Physiol.*, **236**, C139 (1979).
- (73) L. E. Gerlowski and R. K. Jain, "Pharmacokinetics of Trace Metals: Zinc and Cadmium," presented at AICHe conference, New Orleans, La., 1981.
- (74) H. L. Gabelnick, R. L. Dedrick, and R. S. Bourke, *J. Appl. Physiol.*, **28**, 636 (1970).
- (75) B. E. Ehrlich, C. Clausen, and J. M. Diamond, *J. Pharmacokinet. Biopharm.*, **8**, 497 (1980).
- (76) M. J. Angelo and K. B. Bischoff, "Pharmacokinetics of the Neurotoxin 2,5-Hexanedione: Distribution, Elimination and Model Prediction," presented at AICHe conference, New Orleans, La., 1981.
- (77) J. J. Boylan, J. L. Egle, and P. S. Guzelian, *Science*, **199**, 893 (1978).
- (78) P. M. Bungay, R. L. Dedrick and H. B. Mathews, *J. Pharmacokinet. Biopharm.*, **9**, 309 (1981).
- (79) D. S. Schultz and W. M. Deen, personal communication.
- (80) M. W. Anderson, T. E. Eling, R. J. Lutz, R. L. Dedrick, and H. B. Mathews, *Clin. Pharmacol. Ther.*, **22**, 765 (1977).
- (81) R. J. Lutz, R. L. Dedrick, H. B. Mathews, T. E. Eling, and M. W. Anderson, *Drug Metab. Dispos.*, **5**, 386 (1977).
- (82) D. B. Tuey and H. B. Mathews, *Drug Metab. Dispos.*, **5**, 444 (1977).
- (83) F. K. Dietz, M. Rodriguez-Giaxola, G. J. Traiger, V. J. Stella, and K. J. Himmelstein, *J. Pharmacokinet. Biopharm.*, **9**, 553 (1981).
- (84) L. I. Harrison and M. Gibaldi, *J. Pharm. Sci.*, **66**, 1138 (1977).
- (85) L. I. Harrison and M. Gibaldi, *J. Pharm. Sci.*, **66**, 1679 (1977).
- (86) R. L. Dedrick and D. D. Forrester, *Biochem. Pharmacol.*, **22**, 1133 (1973).
- (87) J. L. Rheingold, R. E. Lindstrom, and P. K. Wilkinson, *J. Pharmacokinet. Biopharm.*, **9**, 261 (1981).
- (88) P. M. Bungay, R. L. Dedrick, A. M. Guarino, *J. Pharmacokinet. Biopharm.*, **4**, 377 (1976).
- (89) C. N. Chen, D. L. Coleman, J. D. Andrade, and A. R. Temple, *J. Pharm. Sci.*, **67**, 38 (1978).
- (90) B. Montandon, R. J. Roberts, and L. J. Fischer, *J. Pharmacokinet. Biopharm.*, **3**, 277 (1975).
- (91) R. H. Luecke and W. D. Wosilait, *J. Pharmacokinet. Biopharm.*, **7**, 629 (1979).
- (92) M. Mintun, K. J. Himmelstein, R. L. Schroder, M. Gibaldi, and D. D. Shen, *J. Pharmacokinet. Biopharm.*, **8**, 373 (1980).
- (93) P. Hekman and C. A. M. van Ginneken, *J. Pharmacokinet. Biopharm.*, **10**, 77 (1982).
- (94) K. J. Himmelstein, I. Guvenir, and T. F. Patton, *J. Pharm. Sci.*, **68**, 435 (1979).
- (95) V. H. L. Lee and J. R. Robinson, *J. Pharm. Sci.*, **68**, 673 (1979).
- (96) S. C. Miller, K. J. Himmelstein, and T. F. Patton, *J. Pharmacokinet. Biopharm.*, **9**, 653 (1981).
- (97) R. K. Jain and J. Wei, *J. Biogeng.*, **1**, 313 (1977).
- (98) R. B. Bird, W. E. Stewart, and E. N. Lightfoot, "Transport Phenomena," Wiley, New York, N.Y., 1960.

- (99) E. F. Leonard and S. B. Jorgensen, *Annu. Rev. Biophys. Bioeng.*, **3**, 293 (1974).
(100) R. K. Jain, J. M. Weissbrod, and J. Wei, *Adv. Cancer Res.*, **33**, 251 (1980).
(101) R. K. Jain, in "Advances in Transport Processes," vol. 3 Wiley, New Delhi, 1983, pp. 205-339.
(102) R. K. Jain, in "Hyperthermia in Cancer Treatment," F. K. Storm, Ed., G. K. Hall, Boston, Mass., 1983, Chap. 2, pp. 9-46.
(103) R. A. Bender and R. L. Dedrick, *Cancer Chemother. Rep.*, **59**, 805 (1975).

ACKNOWLEDGMENTS

This work was supported by grants from the National Science Foundation and the American Cancer Society, an NIH predoctoral traineeship (LEG), and an NIH Research Career Development Award (RKJ).

The authors wish to thank Dr. Robert Dedrick for his helpful comments.

RESEARCH ARTICLES

Dose-Dependent Pharmacokinetics and Biliary Excretion of Bromophenol Blue in the Rat

ROBERT J. WILLS*, RANDALL B. SMITH‡, and GERALD J. YAKATAN*§

Received December 31, 1981, from the Drug Dynamics Institute, College of Pharmacy, University of Texas at Austin, Austin, TX 78712. Accepted for publication August 26, 1982. Present addresses: *Department of Pharmacokinetics and Biopharmaceutics, Hoffmann-La Roche, Nutley, NJ 07110; †Clinical Bioavailability Unit, The Upjohn Company, Kalamazoo, MI 49001; §Warner-Lambert/Parke-Davis, Pharmaceutical Research Division, Morris Plains, NJ 07950.

Abstract □ Concentrations of bromophenol blue (I) in plasma, urine, and bile were determined spectrophotometrically after intravenous bolus injections and infusions in rats. The plasma concentrations were found to decrease monoexponentially after all doses except the highest, where the decrease was biexponential. Although the disposition kinetics of I were apparently first-order at all doses, the half-life increased with increasing dose. The area under the plasma concentration-time curve ($AUC_{0-\infty}$) increased disproportionately with increasing dose. The binding of I to rat plasma proteins, as determined by equilibrium dialysis, showed that the fraction bound (96%) remained constant in the concentration range of 10-300 $\mu\text{g/ml}$. Plasma concentrations were determined at time zero after intravenous administration and after a second dose administered 20 min later when plasma concentrations from the first dose were minimal. The apparent first-order elimination rate constant for the plasma concentration decline following the second dose was significantly less than after the first dose, indicating that the residual dye in the liver altered the elimination of I after the second dose. The fraction of the dose in the liver decreased with increasing dose, indicating a saturable uptake process. The biliary excretion profile reflected the uptake saturation that occurred in the liver and demonstrated that the biliary excretion of I depended on the amount present in the liver. When liver damage was induced by exposure to carbon tetrachloride, dye concentrations in the plasma, liver, and kidney increased markedly.

Keyphrases □ Bromophenol blue—in rat urine, plasma, and bile, dose-dependent pharmacokinetics, biliary excretion □ Pharmacokinetics—bromophenol blue, rat plasma, urine, and bile, biliary excretion □ Biliary excretion—bromophenol blue, rat urine, plasma, and bile, dose-dependent pharmacokinetics

Bromophenol blue (I) is a high molecular weight anionic sulfonephthalein dye (670 g/mole, pK_a 4.0). Several reports (1-3) have shown that I is extensively excreted in the bile and is not metabolized in a variety of species including the rat.

Takada *et al.* (4, 5) conducted studies aimed at characterizing the role of the intracellular protein fractions Y

and Z in the uptake and transport of I in rat hepatocytes, and also developed a linear pharmacokinetic model for the biliary excretion of I after intravenous administration in rats (6). The model adequately described a single low-dose plasma and bile profile, but could not describe the observed nonlinearity at higher doses. The overall aim of these authors was to evaluate I as a model organic anionic compound by characterizing the pharmacokinetics at three different doses. Their report did not fully characterize the pharmacokinetics at any dose. Liver concentrations and plasma protein binding were not measured, and the observed nonlinearity was not addressed.

Studies on the pharmacokinetics of drugs excreted in the bile have increased in recent years as investigators have become more interested in the effects of liver disease on drug clearance, the effects of first-pass liver clearance on drug bioavailability, the effects of enterohepatic recirculation on drug disposition, and the nonlinear excretion of drugs (7-11). Usually these studies have not considered the extent of protein binding, liver-to-plasma and bile-to-liver drug concentration ratios, hepatic blood flow, and bile flow. These factors contribute to the interpretation of hepatobiliary elimination. In addition, the interpretation has been complicated by the use of compounds such as sulfobromophthalein that undergo metabolism. Ideally, a model compound used in studying hepatobiliary elimination would not undergo metabolism, nor enterohepatic recirculation, and would not be pharmacologically active.

The organic anion, bromophenol blue (I), possesses these qualities (2, 4). Therefore, the present investigation was undertaken to: (a) determine the pharmacokinetic profile